A SURVEY OF LASER DIAGNOSTIC TECHNIQUES FOR COMBUSTION MEASUREMENTS

SUBMITTED BY

ROGER A. LUCHETA

IN FULFILLMENT OF THE REQUIREMENT FOR
OPTI 909, UNIVERSITY OF ARIZONA

20 NOVEMBER 2015

Table of Contents

ABSTRACT

This report is a survey of the use of laser-based instrumentation to make measurements of temperature, species concentration, velocity, and particle size and concentration in gas-phase combustion and in gas dynamics, with the emphasis being on combustion. The measurements are interpreted as applications of elastic scattering, inelastic scattering, and interferometry. Limitations of each technique are discussed.

NOMENCLATURE & SYMBOLS

The following lists all of the symbols used in this document. The symbols are given first, in alphabetical order. If a symbol has different uses in different chapters, the chapter for each meaning is specified. The definition follows next, followed by the units of measure in the SI system. Finally, the section in which the symbol is first used in each chapter is given.

SYMBOL	DEFINITION	UNITS (SI)	FIRST OCCURRENCE
Roman alphabet			
a	Radius of a scattering object	[m]	(2.1.1)
a_i	The i'th selected particle radius analyzed in the Malvern sizer	[m]	(2.2.1)
a,b,d	Arbitrary constants used in equations	[n/a]	(3.2.3)
A_{ab}	Einstein A coefficient for the transition a→b	[1/sec]	(3.3.2.1)
B_{ab}	Irradiance-based Einstein B coefficient for the transition a→b	[m^2/J]	(3.3.2.1)
B	Rotational constant of a molecule	[J]	(3.3.1)
c	Speed of light	[m/sec]	(3.3.3), (4.1.1.1)
C(θ)	Scattering coefficient	[0]	(2.1.3)
C_{IJ}	Ratio of the I polarized component of scattered light to the J polarized component of incident light, where I and J can be "horizontal" or "vertical"	[0]	(2.2.2)
E	Electric field strength	[V/m]	(2.1.1), (3.2.3)
E, E_0	Magnitude of an electromagnetic wave	[V/m]	(4.1.1.1)
E_L	Irradiance of a laser beam before scattering	[W/m^2]	(3.3.1)
$E_{theoretical}(i)$, $E_{measured}(i)$	Electric field strength at the i'th ring of a Malvern sizer	[V/m]	(2.2.1)
f (ch. 2)	Focal length of the Fourier transform lens in a Malvern sizer	[m]	(2.2.1)
f_1 , f_2	Factors in adjustment of virtual particle density to real particle density	[0]	(2.1.5)
$F_v(J)$	Rotational energy of a molecule in the J'th rotational quantum state with internal vibration in the ν'th quantum state	[J]	(3.3.1)
f (ch. 2, 4)	Cyclic frequency of a scattered wave	[cycles/sec]	(2.3.3)
G(ν)	Energy of an oscillator in vibrational quantum state ν	[J]	(3.3.1)
g_i	Degeneracy; the number of different quantum states which have the same energy ε_i	[0]	(3.3.1)
h	Planck's constant	[J-sec]	(3.2.4.3)
I	Irradiance (incorrectly called intensity) of a laser beam	[W/m^2]	(3.2.4.3)

I_a	Measured irradiance of a rotational transition between state a and the ground state	[W/m^2]	(3.3.1.2)
I_{pump}, I_{probe}, I_{signal}	The irradiance of the pump beams, the probe beam, and the reflected signal beam in DFWM	[W/m^2]	(3.2.4.3)
$I_S(0)$	Saturation irradiance at the center of a spectral line in DFWM	[W/m^2]	(3.2.4.3)
J_ν, Y_ν	Bessel functions of the first and second kind of order ν	[0]	(2.1.5)
J, J_a	Rotational quantum number, rotational quantum number of state a	[0]	(3.3.1)
K	Wave number	[m^{-1}]	(2.1.3)
k_B	Boltzmann's constant	[J/K]	(3.3.1)
k_1 , k_0 ,K	Incident wave vector, scattered wave vector, interference wave vector in Rayleigh scattering	[m^{-1}]	(2.3.3)
$\vec{k}$	Wave vector	[m^{-1}]	(3.2.3)
$\lvert\vec{k}\rvert$	Wave vector amplitude	[m^{-1}]	(3.2.3)
ℓ	Length of laser beam viewed by optical system	[m]	(2.3.2)
l	Index used in a summation	[0]	(3.2.3)
L	Distance along a coherent scattered wave	[m]	(3.2.3)
n, m	Index of refraction	[0]	(2.1.5) (3.2.4.2)
n_i	Index of refraction of species i at STP	[0]	(2.3.2)
n*(x)	"Virtual" particles per unit volume of particles of dimensionless size x	[m^{-3}]	(2.1.5)
n(x)	Actual particles per unit volume of particles of dimensionless size x	[m^{-3}]	(2.1.5)
N	Particles per unit volume	[m^{-3}]	(2.1.3), (3.2.4.3)
N_i	Molecules per unit volume of species i at STP	[m^{-3}]	(2.3.2)
n_i	Number density of species or state i	[m^{-3}]	(3.3.2.2)
N_0^a	Initial concentration in state a	[m^{-3}]	(3.3.2.1)
$N_a(I_a)$	Number density or density ratio in rotational state a as derived from radiance I_a	[m^{-3}]	(3.3.1.1)
N_m, N_n	Density of molecules in energy state m, n	[m^{-3}]	(3.3.1)
$N_{\nu,J}$	Density of molecules in vibrational energy state ν and rotational energy state J	[m^{-3}]	(3.3.1)
N_σ	The number of zero crossings in a velocity measurement	[0]	(4.2.3)
P	Polarization density	[C/m^2]	(3.2.3)
P_{laser}, P_{Ray}	In Rayleigh scattering – incident laser power, scattered Rayleigh power	[J/sec]	(2.3.2)
P_i , P_r	In Raman scattering – incident laser power, scattered Raman power	[J/sec]	(3.3.2.2)
q_i	The number of Doppler cycles in the *i*-th velocity measurement of a group of velocity measurements at the same point	[0]	(4.2.3)

Q_{ext} (m,x)	Extinction efficiency - ratio of absorption cross-section to physical cross-section	[0]	(2.1.5)
R	Ratio of scattering to attenuation	[C/(m-V)]	(2.1.3)
$R(\tau), R(\tau,\vec{x},\vec{r})$	Correlation functions	[m^2/ sec^2]	(4.2.4)
s	An electronic quantum state	[0]	(3.3.1.2)
S, S_n	Scattering coefficient, n'th scattering coefficient	[0]	(2.1.1)
S_i	Radius of Fraunhofer diffraction ring in Malvern sizer corresponding to particles of radius a_i	[m]	(2.2.1)
T(i,j)	The E field magnitude at Fraunhofer ring i of a Malvern sizer created by a unit density of particles of size a_j	[V-m^2]	(2.2.1)
T	Temperature	[K]	(3.3.1)
T_1, T_2	Decay time of excitation of electronic state; decay time of induced polarization	[sec]	(3.2.4.3)
t	Time	[sec]	(3.2.3), (4.1.1.1)
δt_i	The length of time during which a particle used to make the *i* – th velocity of a group of velocity measurements is giving a scattered Doppler signal	[sec]	(4.2.3)
t_i	The starting time relative to a specified basis of the signal burst defining the *i*-th velocity measurement of a group of velocity measurements at a given point	[sec]	(4.2.4)
u	Velocity of flow, velocity of particle in a flow	[m/sec]	(2.3.3), (4.1.1.1)
u'	Velocity fluctuation about a mean	[m/sec]	(4.2.3)
u_i	The *i*-th velocity measurement of a group of velocity measurements at the same point	[m/sec]	(4.2.3)
u_i'	The fluctuation of the *i* -th velocity measurement around the mean velocity	[m/sec]	(4.2.3)
U	Velocity-weighted average velocity of a collection of velocity measurements at the same point	[m/sec]	(4.2.3)
V	Volume of small particle	[m^3]	(2.1.3)
W(j)	Particle number density of particles of size a_j	[m^{-3}]	(2.2.1)
w	Fringe spacing in an LDA measuring volume	[m]	(4.1.2.2)
x (ch. 2)	Ratio - (particle circumference)/(illuminating wavelength)	[0]	(2.1.1)
x (ch. 4)	Distance along the travel of a particle in flow	[m]	(4.1.1.1)
z	Distance along a coherent scattered wave	[m]	(3.2.3)
Z	Partition function	[0]	(3.3.1)
Greek alphabet			
α	Polarizability of small particle	[C-m^2/V]	(2.1.3)
α_i	Depolarization ratio of species i	[0]	(2.3.2)

δ	Angle between flow velocity and local fringe line	[radian]	(2.3.3)
ε (ch. 2.1)	Permittivity	[C/(V-m)]	(2.1.3)
E (ch. 2.3)	Efficiency of an optical system	[0]	(2.3.2)
ε_i	Energy of a quantum state	[J]	(3.3.1)
ε_0	Permittivity of free space	[C/(V-m)]	(3.2.3)
Ω	Solid angle of optical system as viewed from scatterer	[sr]	(2.3.2)
θ (ch. 2)	Scattering angle	[radians]	(2.1.1)
θ, θ' (ch. 3)	Angles between wave vectors in coherent Raman spectroscopy	[radians]	(3.2.3)
θ (ch. 4)	Angle between intersecting beams of laser light	[radians]	(4.1.1.1)
λ	Wavelength of light	[m]	(2.2.1) (3.2.4.2) (4.1.1.1)
μ_{12}	Dipole moment	[C-m]	(3.2.4.3)
ν (ch. 3)	Vibrational quantum number of an oscillator	[0]	(3.3.1)
ν_s, ν_{as}	Center frequency of Stokes, of anti-Stokes wing of spectrum	[1/sec]	(3.3.1.1)
$\Delta\nu$ (ch. 3)	Difference between center frequencies of Stokes and of anti-Stokes wings	[1/sec]	(3.3.1.1)
ν,$\Delta\nu$ (ch. 4)	Cyclic frequency, cyclic frequency shift of an optical wave in a LIF velocity measurement	[cycles/sec]	(4.1.1.5)
σ_f	Broadening of a Doppler velocity spectrum due to finite length measurement	[radian/sec]	(4.2.3)
τ	The time difference in a correlation function	[sec]	(4.2.4)
Φ_s, Φ_{as}	Integrated area of Stokes, anti-Stokes wing of spectrum	[J/sec]	(3.3.1.1)
Φ – (ch. 2)	Angle between incident and Rayleigh scattering direction in the scattering plane	[radian]	(2.3.2)
Φ - (ch. 3)	Scattered power collected by optical system	[J/sec]	(3.3.1)
χ_i	Mole fraction of species i	[0]	(2.3.2)
$\chi(\omega)$	Susceptibility	[0]	(3.2.3)
$\chi^{(n)}(\omega)$	n'th order term of nonlinear susceptibility	$[(m/V)^{(n-1)}]$	(3.2.3)
ω	Angular frequency	[radian/sec]	(3.2.3) (4.1.1.1)
$\delta\omega$	Imposed shift in optical wave angular frequency by Bragg cell or comparable device	[radian/sec]	(4.1.1.3)
ω_d	Doppler frequency of a velocity measurement	[radian/sec]	(4.1.2.2)
ω_D	Mean Doppler frequency of a Doppler velocity spectrum	[radian/sec]	(4.2.3)
$\left(\frac{\partial\sigma}{\partial\Omega}\right)_i$	Scattering cross-section for species i	$[m^2/sr]$	(2.3.2)
Subscripts			
$()_h$	Horizontally (in plane) polarized component	[na]	(2.1.1)

$()_{\mathbf{v}}$	Vertically (out of plane) polarized component	[na]	(2.1.1)
$()_{\mathbf{a}}$, $()_{\mathbf{b}}$, $()_{\mathbf{1}}$, $()_{\mathbf{2}}$	Arbitrary designators used in deriving equations	[na]	(3.2.3)
$()_{\mathbf{i}}$	A specified quantum state	[na]	(3.3.1)
$()_{\mathbf{p}}$, $()_{\mathbf{q}}$	Designators for two different quantum energy levels	[na]	(3.3.1)
$()_{\mathbf{Ray}}$	Related to Rayleigh scattering	[na]	(2.3.2)
$()_{\mathbf{s}}$	Saturation value	[na]	(3.2.4.3)
$()_{\mathbf{d}}$	Doppler	[na]	(4.1.2.2)
$()_{\mathbf{D}}$	Doppler	[na]	(4.2.3)
$()_{i}$	Enumerator of one of a group of velocity measurements	[na]	(4.2.3)

1. INTRODUCTION, BACKGROUND, AND JUSTIFICATION

1.1 PURPOSE

This document is a survey of the optical science and the modern optical techniques used in combustion science and engineering. It is intended to give someone unfamiliar with the field the ability to understand, in some detail, the underlying operation and mechanisms of the techniques. Laser techniques are emphasized, because, in the last few decades, the rapid evolution of laser technology has given the experimenter a continuous stream of potent tools which can be applied to combustion measurements.

1.2 ORGANIZATION

The primary organization of this document is into three groups of phenomena which seem to span the techniques used. These are: 1) Elastic scattering; 2) Inelastic scattering; 3) Interferometry. Within each of these groups, relevant combustion parameters are identified, and the means of optically measuring them described. The emphasis is on gaseous combustion since, with one notable exception - the oxidation of solid carbon to carbon monoxide - all practical combustion processes ultimately take place in the gas phase.

1.3 COMBUSTION, ITS SIGNIFICANCE, AND ITS VARIATIONS

1.3.1 Definition and Significance of Combustion

First of all, we define combustion, adapting from Ref. 1, p. 6, as "Rapid oxidation, generating heat, or both light and heat". In most applications, the heat is the desired product, either in and of itself, or for conversion to mechanical energy. Combustion can also be used to perform desired chemical reactions. These are usually destructive, such as the destruction of hazardous chemicals, but some syntheses – such as creation of diamond-like carbon – have also been performed.

The significance of combustion need not be belabored – from the time of the cave man and in the primitive world, combustion was seen as a gift of the gods, allowing humanity to rise above the level of the beasts. At that time, and into the modern age, the main emphasis of combustion studies was on how to use combustion as intensely and broadly as possible, with little thought of adverse environmental effects, and with the only limitations on use being limitations on the acquisition of the fuels. Perhaps the ultimate expression of combustion research 50 years ago was research in rocket propulsion, which emphasized the development of techniques for the most intense release of energy, with no thought of limitations on the availability of propellants, of their environmental results, or of their effects on health.

At present, over 80% of the energy used in the United States results from combustion, either directly or indirectly. An example of an indirect use is electricity generated by burning fossil fuels – coal, natural gas, etc. Many power sources which are thought of as not relying on combustion ultimately do – for instance, a hydroelectric dam may be made of concrete, whose

cement component was calcined in a combustion-heated kiln; similarly, solar cells rely on zone-refined silicon, where the electric heating for the zone refining probably came from a coal-fired power plant. Today, the benefits of combustion are being overshadowed, in the public mind, by its negatives – scarcity of fuels, the geopolitical impact of the distribution of fuel sources, and the adverse environmental effects of burning of the fuel. Research and engineering have shifted to the development of techniques for the economical use of fuels, with minimum environmental impact.

1.3.2 Variations of Combustion

Combustion takes place under an almost infinite variety of circumstances – indeed, even stellar phenomena have been interpreted with a combustion paradigm (Ref. 2). Some of the variations which will be encountered here are:

1) Turbulent combustion, in which there are spatial and temporal fluctuations in the flow patterns that are so small and/or so rapid that they must be accounted for statistically;
2) Laminar combustion, in which the flow of gases varies sufficiently slowly, spatially and temporally, that the variations can be tracked in detail ;
3) Premixed combustion, in which reactants are mixed before ignition;
4) Diffusive combustion, in which the reactants mix while burning;
5) Subsonic combustion, in which all velocities in the reacting flow field are slower than the local speed of sound;
6) Supersonic combustion, in which some or all velocities in the reacting flow field are faster than the local speed of sound.

The difference between "turbulent" (item 1) and "laminar" (item 2) is somewhat arbitrary, being a matter of the spatial and temporal resolutions available. If the time and spatial scales chosen are sufficiently small, everything becomes unsteady laminar; if sufficiently large time and distance scales are chosen, everything is described by statistics, and is turbulent.

1.4 WHY LASERS?

Prior to the development of the technology described in this survey, measurements were made by the insertion of various probes into the flow, by the spectroscopic analysis of emissions from the flame, and by photographic methods to measure density using schlieren, interferometry, or shadowgraphs.

Probe techniques were highly developed (Ref. 3), but always suffered from the inherent weakness that they interacted with the flow, and, in so interacting, gave an altered reading. The interactions could be thermal, physical, or chemical. An example may clarify this. It would seem simple to measure the temperature of a gas by sticking a thermocouple into it and reading out the temperature. The problem is that the thermocouple, when heated to the measurement temperature, is partially cooled by giving off thermal radiation, and so comes to a temperature at which it is at equilibrium between the heat given off by radiation and the heat absorbed from the gas – a difference which can easily be hundreds of degrees. In extreme cases, when measuring temperature in an enclosed combustion chamber with slow-moving gases, the temperature read

by the thermocouple might result from a radiative balance with the walls, and have no relationship to the gas temperature at all. The thermocouple can also catalyze reactions on its surface, leading to artificially high temperature readings. Comparable problems arise with probes for velocity and for species measurements.

Techniques using the measurements of the emissions from flames were similarly highly developed (Ref. 4), but gave the experimenter no control over what was observed – if a spectroscopic feature was not naturally present, there was no way to stimulate it to probe its nature.

Photographic techniques also had been highly developed (Ref. 5), but suffered from the fact that they inherently gave a measurement which was integrated over a path length, and so had limited spatial resolution. It was possible to build useful experimental setups – such as a square detonation tube - which were relatively uniform along the path length for research purposes. However, practical combustion devices are not amenable to such analysis.

Chigier (Ref. 6, ch.10) gives a list of the advantages of laser measurements, as follows:

1) Visible laser beams experience negligible attenuation in combustion unless there is a high concentration of particulates;
2) The laser beams cause no perturbation or disturbance to the system;
3) The coherence of laser light allows focusing of the beams on small measurement volumes;
4) Measurements can be made at large distances from the laser;
5) Radiation from the flame can be excluded by the use of spatial and narrow-band spectral filtering.

Ref. 24, ch. 1 adds the following:

6) Laser measurements can be used to measure very high-frequency fluctuations in flow, and very short-lived, unstable chemical species;
7) Often velocity, temperature, and chemical species measurements can be made simultaneously, allowing exploration of the relationships between these.

1.5 ORGANIZATION OF THIS SURVEY

As mentioned previously, this survey is organized by three classes of optical phenomena for which laser techniques have been used to make measurements in flames. These are:

1) Elastic scattering, used to measure particle sizes by Mie scattering, and density, temperature, and velocity by Rayleigh scattering;
2) Inelastic scattering, used to measure chemical species and temperature by molecular spectroscopic techniques;
3) Interferometry, used to measure velocities by Doppler-shifted scattering.

2. ELASTIC SCATTERING - MIE SCATTERING AND VARIATIONS ON MIE SCATTERING

2.1 INTRODUCTION – THE BASIC PHENOMENON

2.1.1 Basics of Particulate Scattering

Two crucial parameters in combustion involve the measurement of the size of small particles. These are: 1) The measurement of the size of soot particles, - in particular the growth of these particles from their genesis as large molecules to their final size as colloidal or larger particles, and; 2) The measurement of fuel droplet sizes in fuel sprays preparatory to combustion. Laser techniques have brought a versatility and precision to these measurements which was not available before, but the fundamentals of such measurements go back a long time.

The scattering of light by small objects, and the use of the properties of this scattering to infer the size of the objects, was initiated with the "Eriometer" in 1790 (Ref. 22). This device determined the size of wool fibers from the size of the colored diffraction rings of light transmitted through a bundle of fibers. 140 years later, a quite sophisticated analysis (Ref. 21) determined that the instrument was as good as were modern microscopic techniques.

Lord Rayleigh's classical analysis of light scattering began the rigorous scientific study of the subject. This analysis assumed that the scattering particle was much smaller than the wavelength of the light being scattered, and also was a pure dielectric, with no dissipation. The analysis requires that the particle be so small that the electric field that the particle experiences is uniform over the entire volume of the particle. The re-radiated light from every point of the surface has the identical phase. The model implicitly assumes that there is no phase shift between the incident light and the induced polarization, unlike the Lorentz oscillator model which does allow for such a phase shift to arise.

The more general problem of the scattering of a plane wave by a spherical particle of arbitrary size, having complex permittivity, was solved by Gustav Mie. Solutions are replicated in Refs. 7 and 8, and the details of how the solutions are obtained need not concern us here. It should be noted that use of the final formulae involves the calculation of infinite series of Bessel functions of fractional order with complex arguments.

The Mie scattering analysis gives the relationship between a plane wave, incident on a spherical particle, and the far-field scattered wave. In order to understand how the solutions are applied, we first use Fig. 2.1 to review the conventions and terminology used in Mie scattering.

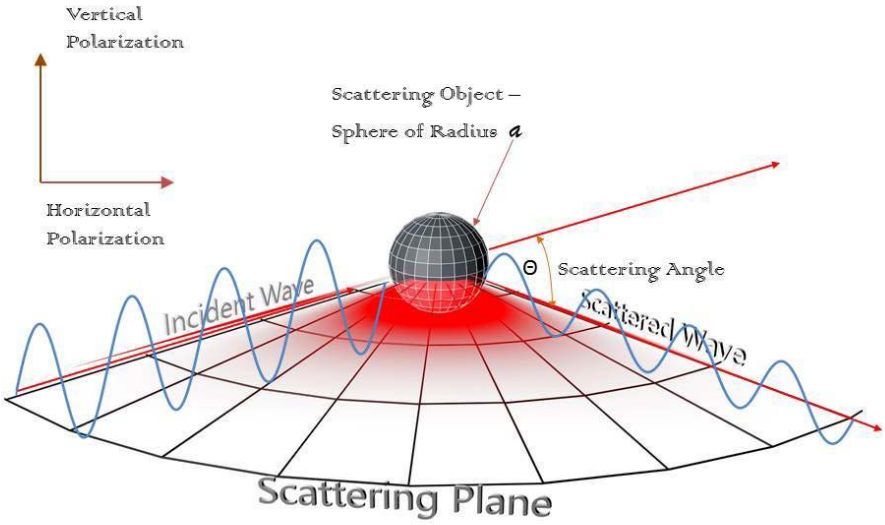

Fig. 2.1 – Scattering Geometry – Description Follows

The "scattering plane" is a plane in which the incident wave vector and a wave vector of the scattered wave are coplanar. This is an artifice created for the analysis – due to the symmetry of the situation, the scattered light is not restricted to a single plane, but referencing the description and analysis to such a plane is convenient for purposes of analysis, and in no way restricts the generality of the result obtained. The direction of the scattered wave, or "scattering direction", would more correctly be referred to as the "observation direction".

The "scattering angle" is the angle between the direction of the incident wave vector and the direction of the scattered wave vector, at the point of observation.

"Vertical" or "perpendicular" polarization is polarization such that the electric vector is perpendicular to the scattering plane, which plane is defined by the choice of direction of observation.

"Horizontal" or "parallel" polarization is polarization such that the electric vector lies in the scattering plane, which plane is defined by the choice of direction of observation.

It should be observed that whether a polarization is described as "vertical" or "horizontal" does not arise from the inherent nature of the light, but rather arises from the orientation of the polarization with respect to the chosen plane of observation.

Both the incident wave and the scattered wave can have vertical and horizontal components of polarization – in the situation described by the basic Mie analysis, the vertical component of the incident wave will elicit only a vertical component of the scattered wave, and the same for the horizontal components of the incident and scattered waves.

The relationship can be written as a matrix equation relating the horizontally – $()_h$ - and the vertically – $()_v$ – polarized components of the scattered E vector to the incident components of the E vector:

$$\begin{pmatrix} E_h \\ E_v \end{pmatrix} = \begin{pmatrix} S_2 & S_3 \\ S_4 & S_1 \end{pmatrix} \bullet \begin{pmatrix} E_{h0} \\ E_{v0} \end{pmatrix} \qquad (2\text{-}1)$$

The *S* terms are functions of only the scattering angle - θ - and of the index of refraction – *n* – of the sphere, remembering that the index of refraction is usually a complex number. In the case of the Mie analysis, $S_4 = S_3 = 0$.

The complex relative permittivity, which is the square of the index of refraction, is also used in analyses, as is the complex permittivity which is the complex relative permittivity multiplied by the square of the permittivity of free space.

If we are looking only at a single, perfectly spherical particle, then a series of measurements of the scattered light intensity as a function of scattering angle – $S(\theta=0)$, $S(\theta=\theta_1)$, $S(\theta=\theta_2)$ . . . $S(\theta=\theta_k)$, will be unique to only a single radius – *a* – and a single complex refractive index - *n*. The *S* can be either S_1 or S_2. One important point made in Born and Wolf (Ref 11, p. 759) is that "the solution due to Mie, though derived for diffraction by a single sphere, also applies to diffraction by any number of spheres . . . Under these circumstances, the total scattered energy is then equal to the energy that is scattered by one sphere multiplied by their total number." While this is encouraging, and would be of great use in evaluating a cloud of perfectly uniform particles, we will see later that things get harder with a cloud of particles of different size. Also, Born and Wolf's statement would break down for a dense cloud of particles such that there is significant secondary scattering, but Ref. 9 presents calculations which show that this is not significant if particle separation is more than 3 particle diameters, which is a much greater density than is normally encountered in combustion applications.

Figure 2.2 (from Ref. 8, p. 152) gives a set of typical curves of scattering magnitude vs. scattering angle for a range of ratios of *x* = (circumference)/(wavelength), from 1.0 at the top to 6.0 at the bottom, and for vertically polarized (solid lines) and horizontally polarized (dashed lines) incident light. As can be seen, as the particle size goes up, the curves have more and more maxima and minima. For very large particles (*x* in the hundreds), the number of fringes per degree is linearly related to the diameter, as shown in Fig. 2.3 (taken from Ref. 10). Indeed, at this point (the "geometric optic" limit) the detailed Mie scattering becomes useless, and a diffraction-based analysis is used instead – as discussed in the "Malvern Sizer" section below. Going to the other extreme, we might suspect that the scattering becomes independent of size for particles much smaller than the wavelength of light, and this is indeed the case discussed in the "Rayleigh limit" section below.

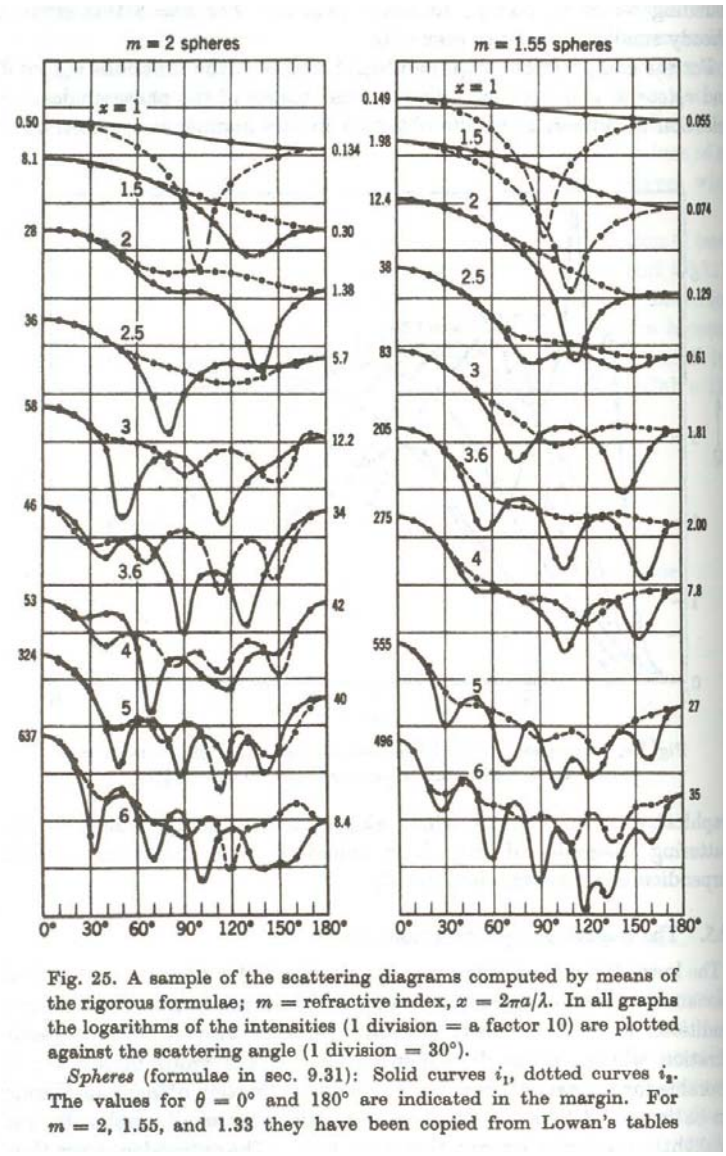

Fig. 25. A sample of the scattering diagrams computed by means of the rigorous formulae; m = refractive index, $x = 2\pi a/\lambda$. In all graphs the logarithms of the intensities (1 division = a factor 10) are plotted against the scattering angle (1 division = 30°).

Spheres (formulae in sec. 9.31): Solid curves i_1, dotted curves i_2. The values for $\theta = 0°$ and 180° are indicated in the margin. For $m = 2$, 1.55, and 1.33 they have been copied from Lowan's tables

Fig 2.2. (from Ref. 8, p. 152) – Scattering Maxima and Minima as Function of Sphere Radius. The horizontal axis is the viewing angle relative to the incident angle. The vertical axis is the irradiance of the observed light. Left and right plots are given for two different indices of refraction; within each plot, solid curves represent horizontally polarized, and dashed curves represent vertically polarized light. The matter of interest here is how the number of lobes increases with the ratio x = (circumference)/(wavelength). Notice that the smallest sizes go to the uniformity of the Rayleigh limit, while the larger sizes show periodicity of the lobes.

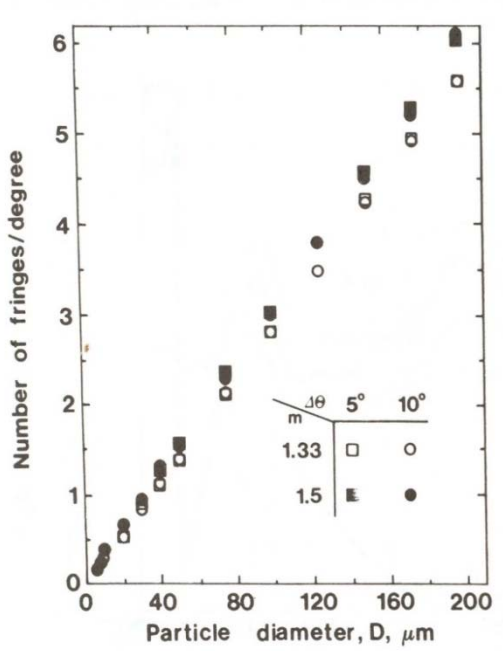

Fig. 2.3 (from Ref. 10, Fig. 9-5) – Fringes per Degree in the Large Particle Limit near Scattering angle of 90°.
Data is given for particles with two indices of refraction – m=1.33 (open points) and m=1.5 (closed points). Wavelength of light is not specified for this curve, but Ref. 10 generally only considers light in the visible range. As can be inferred from Fig. 2.2, the fringes per degree increase as the size of the particle increases. Fringes per degree were measured over two angular intervals - $\Delta\theta = 5°$ (square points) and $\Delta\theta = 10°$ (round points), and can be seen to be very consistent.

2.1.2 Complications

The solid particles in a combustion system differ from the Mie model as follows (in roughly the order of importance that seems to be assigned in the references I searched – including, but not restricted to, Refs. 9, 10, 12, 14, 15, 20, 23):

1) The particles have a range of diameters rather than a single diameter;
2) The complex index of refraction - particularly the imaginary part – is poorly known;
3) Multiple scattering can occur;
4) The illumination is not made of planar beams;
5) The particles are not spherical.

I have found no significant effort applied to item (5) in the relevant combustion literature which I searched (Refs. 19, 20 *inter alia*). This probably arises from two reasons: a) The particles of interest are not seriously elongated, with the exception of agglomerated soot, and; b) The diameter as measured by the Mie scattering is adequate to characterize the mass distribution as a function of "size", which is the matter of greatest interest. While it does create a situation in which S_4, $S_3 \neq 0$, this is often ignored and the spherical particle analysis is used. However, in some analyses, (Ref. 15 notably) these two components are exploited to determine the shape of the particles.

In contrast, items (1) and (2) have attracted extensive analyses. What seems to be the best analysis of item (1) is in Ref. 9. In this, the particle size distribution is characterized as log-normal – common practice for characterizing dusts - with a log-mean and a log-standard deviation. A scattering pattern $S(\theta)$ is then computed as the weighted sum of the scattering patterns of individual particle sizes within the distribution. The mean, the standard deviation, and the complex index of refraction are then adjusted by a least squares fit so that the computed pattern matches the measured pattern. We should note that, if particles are measured one at a time (as discussed below), the size distribution problem goes away.

The problem of the complex index of refraction is dealt with in numerous ways, remembering that the compositions of the particles are not known *a priori*. The simplest way is to assume that the particle has a certain composition, and make refractive index measurements on planar samples of this composition. The next step up is to collect the particles and materials of the same analyses as these particles - or a test plate made up of the particles themselves – to get the refractive index data. For a restricted range of particle sizes, an *in situ* technique using xenon lamp sources was developed by D'Alessio, (Ref. 80) but a close reading of the paper brings out that it requires a reference value of the complex index of refraction. The final step – which has not been too successful to date - is to derive the complex relative permittivity from quantum mechanical calculations based on the electronic structure of the molecules (Ref. 13). An exhaustive search found no follow-up to this approach.

Multiple particles, as in item (3), can be dealt with by having a tightly focused laser beam for illumination, and viewing only a small portion of the beam, dealing with the stringent alignment requirements resulting from this. However, calculations reported in Ref. 9 showed that errors due to multiple scattering are not significant if the particle separation is more than 3 particle diameters. Ref. 9 also shows that particles significantly smaller than the wavelength scatter depending only on their volume, regardless of shape. This will be discussed later.

Item (4) has attracted some really good-quality work. In single-particle measurements, the particles must be precisely located, so that the angular measurements are accurate. In these cases, the scattering measurement is made at the intersection of the waist of a Gaussian beam and the focus of the angular measuring device. But then the particle is no longer illuminated by a single, uniform plane wave, and the intensity depends on where in the beam the particle is. More subtly, since a Gaussian beam can be represented as the intersection of planar beams of different orientations, the scattering angle is no longer clearly defined relative to a uniquely defined incident planar wave. This is addressed in Ref. 10, ch. 10 ("Generalized Lorenz-Mie Theory and Applications to Optical Sizing") by replacing the Fourier representation of the Gaussian beam as the sum of planar waves of different directions. The replacement is achieved by representing the beam in a curvilinear coordinate system matched to the beam. The Mie scattering is computed in this coordinate system, and then converted back to an orthogonal coordinate system.

2.1.3 Extension – Small Particles in the Rayleigh Limit

If the particles are much smaller than the wavelength of light, the Mie scattering formulae become the Rayleigh scattering formulae. The most significant result of this is that the scattering pattern is no longer size-dependent. At this point, it is still possible to use scattering

measurements, to include the idea that the attenuation along the propagation direction of light is still scattering.

The basics of this technique are laid down in Ref. 8, ch. 6 ("Particles Small Compared to the Wavelength"), and are elaborated here. First of all, a parameter – α - is defined which is the polarizability of a particle of volume V, converted from CGS electrostatic units in the original to rationalized MKS here

$$\alpha = (\varepsilon - \varepsilon_0)\cdot V \quad (2\text{-}2)$$

noting that ε is usually a function of wavelength, and can be a complex number. In most cases of interest in combustion, the imaginary part of the permittivity is small. Consider a volume with N particles per unit volume, illuminated by light of a wave number k. Then the ratio of scattered irradiance to the incident irradiance, measured at an angle θ to the direction of the incident beam, is

$$C(\theta)\cdot N\cdot(8\pi/3)\cdot k^4\cdot\alpha^2$$

The constant of proportionality $C(\theta)$ is a function of the scattering angle, with the form of the function depending on the sense of the polarization . For natural light, it is

$$C(\theta) = [1+\cos^2(\theta)]\cdot[3/(8\pi)] \quad (2\text{-}3)$$

For "horizontally" polarized light, only the $\cos^2(\theta)$ factor is used, while, for "vertically" polarized light, the $\cos^2(\theta)$ term is deleted.

The deviation from unity of the refractive index of the medium with suspended particles is

$$(n\text{-}1) = 2\cdot\pi\cdot\alpha\cdot N \quad (2\text{-}4)$$

The ratio of the scattering to the refractive index deviation is

$$R = C(\theta)\cdot (4/3)\cdot k^4\cdot\alpha \quad (2\text{-}5)$$

The volume of the particle then follows - since k and ε are assumed known - as

$$V = 3R/(C(\theta)\cdot 4\cdot k^4\cdot (\varepsilon - \varepsilon_0)) \quad (2\text{-}6)$$

The particle loading – N - can then also be determined from

$$N = \frac{n-1}{2\cdot\pi\cdot V\cdot(\varepsilon-\varepsilon_0)} \quad (2\text{-}7)$$

This is for particles of a single size. Ref 64, pp. 10-5 to 10-6 has the detailed formulae which are used for these calculations in an automated device, when there is a spectrum of particle sizes. The trick here is to use multiple wavelengths, and multiple scattering angles, to extract the particle size distribution.

Of course, there is much more experimental complexity than this. Most importantly, it is necessary to eliminate molecular scattering from the measurements, as well as background and large particle scattering. Further, the complex value of ε must be known at the wavelength being used. Ref. 12 describes how all these are done.

Often, it is not possible to be sure that the permittivity measured on a bulk sample actually represents the permittivity of the individual particle, especially since the detailed chemical composition of the particle may be unknown. Considering soot, which is the primary particulate of interest in combustion measurements, Ref. 13 develops a first principles method of determining the complex permittivity of soot, based on molecular quantum mechanics. As of yet, this approach does not appear to have gone anywhere, if an exhaustive literature search which found nothing is to be taken as conclusive.

2.1.4 Extension - Very Large Particles

This is the situation in which the particle size is much greater than the wavelength of the illuminating light. This is sometimes referred to as the "geometric optic" or "ray optic" limit. For a completely opaque particle, Babinet's principle (Ref. 11, p. 424) suggests that the scattering pattern would be the complement of the Airy pattern for diffraction from a hole of the same projected shape. For the more general case of particles with a complex index of refraction, such as liquid fuel droplets or raindrops giving a rainbow, a ray optic analysis can still be applied to give a pattern which is a modification of the Airy pattern.

2.1.5 Extension of the Large Particle Model to the Full Mie Range

This leaves the situation in which the particle size is comparable to the wavelength of the illuminating light. Of course, the full Mie analysis could be used here, but it is so complex that use of it does not allow much mathematical manipulation. Instead, Fymat (Refs. 17 and 18) has extended the Mie analysis down to particle sizes of about 5 times the wavelength, for refractive indices characteristic of soot and fuel droplets, and developed mathematical techniques for using scattering patterns to derive particle size distributions. A further extension to particle sizes equal to the wavelength (Ref. 16) is somewhat more restrictive on permittivities, requiring that the imaginary part be much less than the real part. While this is probably valid for droplets of transparent liquids, it is certainly not the case for soots, where the imaginary part is about 17% of the real part.

The Fymat analysis was developed over a period of about 20 years. To understand it, we must first remember several concepts about diffraction patterns with changing particle size. We then view the historical development from the original forward scattering model of Hodkinson (Ref. 19) through to the full flowering of the analysis (Ref. 16).

First summarizing the changes in the scattering patterns as we go from particle sizes much less than the wavelength of light to sizes much more than the wavelength of light:

1) As particle size is increased from very small (the Rayleigh limit) to very large (the Fraunhofer or geometric limit) the scattering pattern goes from a single-lobed dipole pattern to an increasingly multilobed pattern, ultimately becoming a Fraunhofer pattern;

2) Going from the Rayleigh limit to the Fraunhofer limit, the forward scattering lobe becomes more prominent, but narrower;
3) In the Fraunhofer limit, the shape of the forward lobe loses its dependence on permittivity, and depends only on (particle size)/(wavelength);
4) In the Fraunhofer limit, the magnitude of the forward lobe is a function of the permittivity and the (particle size)/(wavelength), in the form of a simple multiplier;
5) In the Fraunhofer limit, spherical particle size and diffraction pattern are a Fourier-Bessel transform pair. The far-field diffraction pattern from a particle is the Fourier transform of the particle cross-section. We know that the Fourier transform of a Fourier transform gives us back the original function (with a change of sign of the independent variable) so that particle size and scattering pattern do, indeed, form a Fourier transform pair.

The first step in this development was taken by Hodkinson (Ref. 19). Starting with exact solutions (both Mie and Fraunhofer) of the shape of the forward scattered pattern in the range from 0° to 35°, he found that, for any specific ratio of (particle size)/(wavelength), the shape of the intensity of the lobe was very nearly constant, regardless of the refractive index. Expressed otherwise, the ratio of (intensity at one angle)/(intensity at a larger angle) was a function only of (particle size)/(wavelength).

Unfortunately, Hodkinson's technique could only be used for assemblages of particles of one size. Because this model does not factor in the amplitude of the lobe, and the amplitude still depends on the size and the permittivity, there is an unknown size factor which cannot be taken out if more than one particle size is involved.

To get out of this dilemma, we return to item (5) above. If we were working in the pure Fraunhofer range, a polydisperse cloud of particles would give a diffraction pattern which would be the weighted sum of the diffraction patterns of the individual sizes of particles, or a sum of Bessel functions, provided that the cloud is not so dense that secondary scattering becomes significant. It would then be possible to go back to the size distribution by doing a Fourier-Bessel expansion of the scattering pattern – a mathematical technique of the same type as is used to extract the harmonic content of a complex waveform into constituent pure sinusoids.

Fymat extends this concept by demonstrating that:

1) The particle size distribution and the scattering intensity as a function of angle at a fixed wavelength can be written as a transform pair even outside the Fraunhofer limit – (Ref. 17);
2) The particle size distribution and the attenuation as a function of wavelength at a fixed angle - can also be represented as transform pairs even outside the Fraunhofer limit – (Ref. 18.), and;
3) The effect of permittivity can be factored as a multiplicative factor in both cases.

However, it must be noted that the transforms Fymat derives are much more complex than simple Fourier-Bessel transforms.

The situation in item (1) above – intensity as a function of scattering angle at fixed wavelength - is the most completely developed (Ref. 16, p. 197). It begins with a measured intensity pattern

I(θ) (ratio of scattered radiance to incident radiance) of light with a wave number k, and proceeds first to get a "virtual size distribution" $n^*(x)$ as

$$n^*(x) = -\frac{2\pi k^3}{x^2}\int_0^\infty (x\theta)J_1(x\theta)Y_1(x\theta)\left[\frac{d}{d\theta}\left(\theta^3 I(\theta)\right)\right]d\theta \qquad (2\text{-}8)$$

with J_1 and Y_1 being first-order Bessel functions of the first and second kind. This is then corrected to the true size distribution – $n(x)$ - by factoring in the effect of refractive index – m – and (particle size)/(wavelength) – x – in the form:

$$n(x) = \frac{4n^*(x)}{\left[Q_{ext}^2(m,x)\cdot f_1(m,x)\cdot f_2(m,x)\right]} \qquad (2\text{-}9)$$

where Q_{ext} is the extinction efficiency, and f_1 and f_2 are, themselves, not too messy functions of zeroth order Bessel functions of the first kind.

We have discussed the determination of particle size distribution from the angular variation of scattering intensity at fixed wavelength. The application of Fymat's determination of particle size distribution from variation of wavelength would seem to be highly attractive in a world of tunable lasers, but this seems to have gone nowhere, perhaps because it requires knowing the index of refraction as a function of wavelength.

2.2 MIE SCATTERING – SOOT/DROPLET SIZING

Having described the underlying science, how are these used to measure particle size distributions in combustion systems? The best way is to give examples from the literature.

2.2.1 The Malvern Sizer

The Malvern sizer (Ref. 10, pp. 190-194) was an early application of these concepts to measurements of particle sizes in the "geometric optic" limit, and it serves to illustrate the mathematical concepts. It was based on the assumption that the particle sizes can be put into i bins, each with a specified mean radius a_i. If a cloud of such particles is then illuminated by a parallel beam of wavelength λ and focused on a screen by a lens of focal length f, then the peak intensity of the Fraunhofer diffraction pattern will be at a radius – S – such that

$$S_i = 1.357\cdot\lambda\cdot f/(2\cdot\pi\cdot a_i) \qquad (2\text{-}10)$$

A photodetector (or a ring of photodetectors) was placed at each S_i corresponding to each a_i. Notice that, in reality, the arrangement of the photodetector rings was fixed in the instrument, and the radius a_i corresponding to each ring could be changed by changing the focal length – f – of the "Fourier transform lens".

If a unit density of particles of another size – j – is present, it will create an intensity at ring i which can be computed, and represented as a matrix element - $T(i,j)$. If an actual distribution of densities of the different sizes is present, it can be represented as a column vector $W(j)$, which is

what we wish to determine, so that, in theory, the distribution of intensities at the i rings should be given by the matrix operation:

$$E_{theoretical}(i) = T(i,j)\cdot W(j) \qquad (2\text{-}11)$$

We note that since we have the same number of rings and of bins, $T(i,j)$ is a square matrix.

In actuality, the measured intensities are

$$E_{measured}(i)$$

so that the $W(j)$ can be determined by minimizing the sum

$$\sum [E_{measured}(i) - T(i,j)\cdot W(j)]^2$$

where the summation is over all values of i. While I have found nothing in the literature addressing this, personal experience with other least squares fitting efforts makes me wonder if the number of bins might not prudently be less than the number of rings, to assure a result less subject to roughness due to the unavoidable imprecision of measurements.

The actual construction was as shown in Fig. 2.4, following:

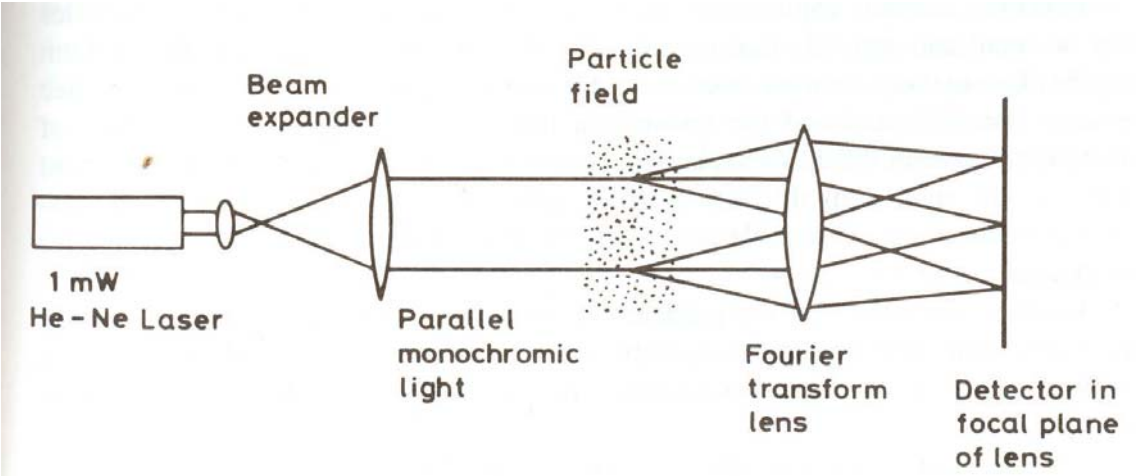

Figure 6-11 Optical setup for laser diffraction technique.

Fig. 2.4 (Ref. 10, Fig 6.11) – Layout of Malvern Sizer.
This instrument exploits the concept, from Fourier optics, that a lens gives the Fourier-Bessel transform, at the focal plane, of an incident pattern of illumination carried by parallel light entering the lens. Thus, by illuminating the particle field with parallel monochromatic light, the pattern on the focal plane will be the sum of the Bessel transforms of the different sizes of particles.

While reference was made to "rings" of photodetectors, one way in which the ring was achieved was to have a single photodetector at each radius, and rotating the plate holding the detectors in the focal plane.

We notice that the lens is placed in the optical path such that the region measured is between the light source and the lens, with the lens between the region being measured and the sensing array. Ref. 62 discusses, this, calling it a "classic" or "forward Fourier" setup, and compares it to a "reverse Fourier" setup, in which the lens is placed between the light source and the region being measured.

The major difference between the two is that the "forward Fourier" arrangement only permits the sensing array to view the forward scattered light, while the "reverse Fourier" arrangement allows sensing of both forward and back scattered light. There is a tradeoff, however, in that the depth of field which can be analyzed by the "forward" arrangement can be much greater than that analyzed by the "reverse" arrangement; the other side of the tradeoff is that the "reverse" arrangement can go to much smaller sizes, and achieves much better resolution.

A prime example of the "reverse" arrangement, called the "Mastersizer 3000" by the developer (Ref. 63), uses a focal plane array, forward and back scatter, large angle measurements, and two wavelengths of illumination, combined with vastly more extensive computational capability, to cover a range of sizes from 20 nm to 3 mm with a single instrument. Such instruments are now considered to be the gold standard of particle size measurement, and are incorporated into an ISO standard (Ref. 61). Notice that the addition of more extensive measuring and computational capability extends the sizing capability well into the Rayleigh range. Unlike the basic Malvern sizer described above, however, measurement can only be made in a very small cell as might be used in a minimally-sized laboratory apparatus, and is completely inapplicable to measurements in an operational system.

A refined "forward" instrument is marketed as the "Spraytec" (Ref. 64), which is more suitable for the type of measurements made in combustion research. The Spraytec uses only 32 detectors, measuring size in a range of 100 nm. to 2 mm, but at a rate of 10 kHz. More importantly, it can accommodate a volume 0.75 meters (≈ 30") deep. The combination of properties make it eminently suitable for measuring the growth and the development of soot and of sprays. Additionally, the vendor claims to have an algorithm which corrects for multiple scattering.

2.2.2 Soot Nucleation Measurements

The nucleation and growth of soot particles in a flame involves particles less than 150 nm diameter, so that here we have a clearly specified Rayleigh limit situation.

Ref. 15 is one of the most nicely documented studies of this sort, using the apparatus as shown in Fig. 2.5 following:

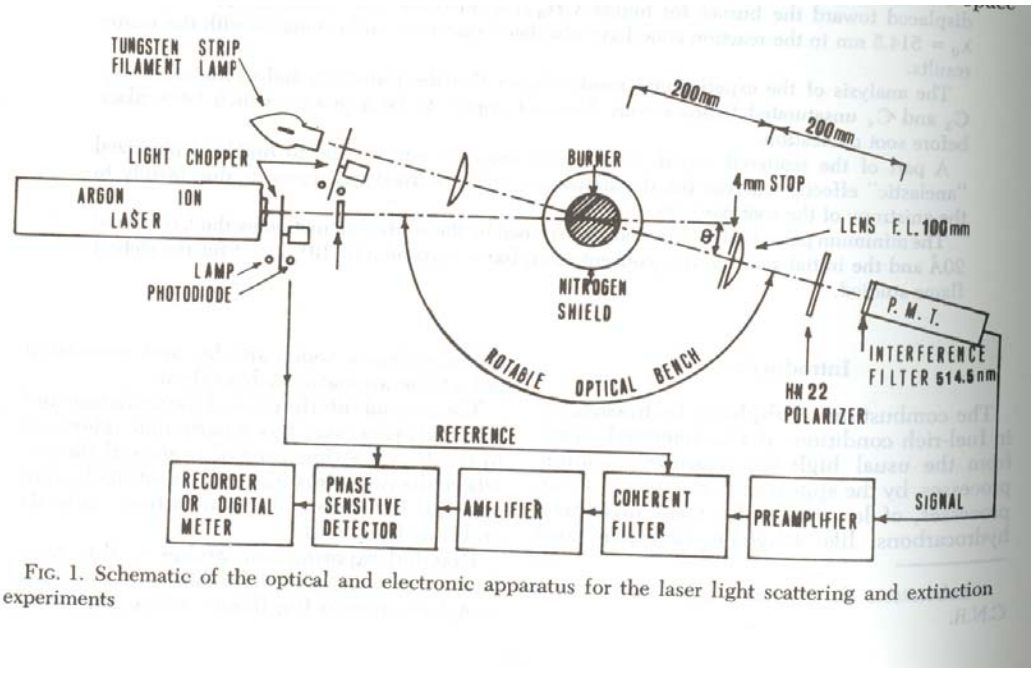

FIG. 1. Schematic of the optical and electronic apparatus for the laser light scattering and extinction experiments

Fig 2 5 – Soot Nucleation Size Measurement Apparatus (figure from Ref. 15, p. 696) Scattering of the beam from the argon laser was measured by the photomultiplier tube, while extinction was measured using the tungsten strip lamp. The various stops and filters assured that the region being investigated was sharply defined.

However, in Ref. 15, the off-diagonal terms in equation 2-1

$$\begin{pmatrix} E_h \\ E_v \end{pmatrix} = \begin{pmatrix} S_2 & S_3 \\ S_4 & S_1 \end{pmatrix} \bullet \begin{pmatrix} E_{h0} \\ E_{v0} \end{pmatrix} \qquad (2\text{-}1)$$

were exploited to get an idea of the departure from sphericity of the soot particles.

At this point, we introduce another notation, often used in the literature, as:

$C_{VV} = S_1$ - The ratio of the vertically polarized scattered light to the vertically polarized incident light;

$C_{HH} = S_2$ – The ratio of the horizontally polarized scattered light to the vertically polarized incident light

$C_{HV} = S_3$; $C_{VH} = S_4$ – Cross polarization ratios of scattered horizontally polarized light to incident vertically polarized light and vice versa – can be shown to be equal.

The significance of the cross-polarization is that it is a measure of the non-sphericity of the particle or molecule – that the cross-polarization components are zero only for symmetrical molecules and soot particles. The volume measurements, as measured by the ratio of scattering to extinction, are independent of the symmetry. The asymmetry of the particles can be determined, in one way or another, by ratios of the off-diagonal to the diagonal elements such as C_{HV} / C_{VV}.

2.2.3 Measurements Based on Full Mie Analysis

Applications of particle size measurement where the full Mie formulation must be used are more scarce. It is mathematically complex to unwrap the combined signal from a cloud of particles of different size, due to the complexity of the Mie scattering pattern. Indeed, Van de Hulst (Ref. 8, p 390) suggests that a physical prefilter procedure be used to reduce the particle size range actually measured, though the Fymat analysis (discussed previously) would appear to offer a way out of this. However, I have found no examples of the Fymat techniques applied to particulate size measurements in combustion or fluid dynamics – its chief usage seems to have been in atmospheric studies.

2.2.4 Measurements Based on Scattering Amplitude

An alternative method, which only uses a minimal amount of scattering theory, relies on measuring the amplitude of the scattered signal, and relating that amplitude to the size of the particle. The instrument is calibrated for scattering intensity at a specific angle with monodisperse particle distribution, and measurements of the polydisperse sample are accumulated particle by particle. The situation is complicated by the fact that, once a tightly focused region is used, the intensity of the scattering depends on where in the beam the particle goes. The way out of this is to get the statistical properties of the scattering patterns of monodisperse sprays in such a beam, and apply these statistics to the measurements (Refs. 81 & 82). Figs. 2.6 and 2.7 illustrate this situation, with Fig. 2.6 showing a scattering measurement, and Fig. 2.7 giving more detail on the nonuniform irradiance in the focal region.

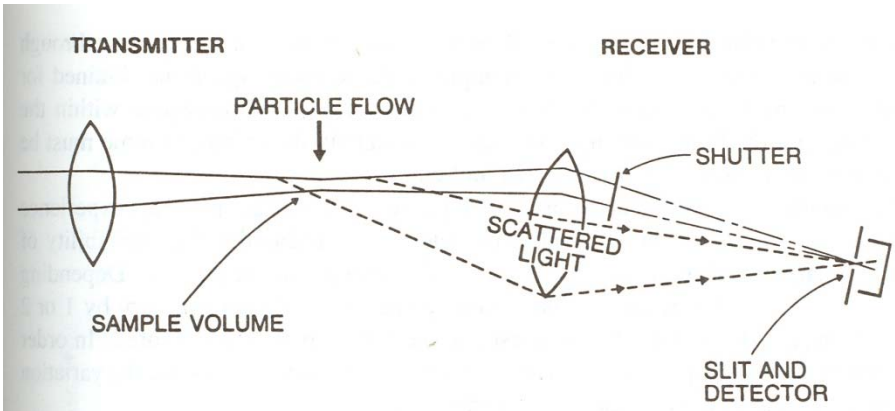

Figure 8-4 Schematic of PCSV sample volume. Focused laser beam and receiver optics define the sample volume.

Fig 2.6 - Sample Volume Illuminated by Gaussian Beam (figure from p. 285 of Ref. 10). The setup is intended to be such that only one particle at a time is in the sample volume and scattering light to the detector. The particular instrument described here infers size from the amplitude of the scattered light, and velocity from the width of the pulse. The difficulty of the techniques arises from the fact that the beam is nonuniform (see comments for Fig. 2.7) and there is no control over where the particle passes through the beam. Refs. 81 & 82 describe how a statistical approach which resolves this problem.

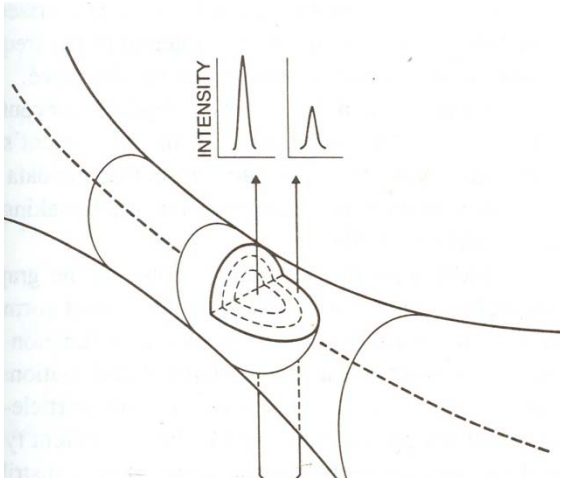

Fig. 2.7 - Sample Volume Illuminated by Gaussian Beam (figure from p. 285 of Ref. 10).
There are two nonuniformities in a Gaussian beam – the obvious one of the variation of amplitude across the beam, and the less obvious one of the variation of direction of the component plane waves determined by Fourier analysis. Both of these complicate analysis of data taken from scattering from particles in the beam. Analyses which depend on variations of amplitude are confounded by the non-uniform amplitude; plane-wave analyses which depend on scattering angles are confounded by the fact that, at any point in a Gaussian beam, there are many plane waves.

2.3 GAS PROPERTY MEASUREMENTS AS THE RAYLEIGH LIMIT

2.3.1 Basics of Molecular Scattering

As mentioned in 2.1.3 above, one of the limiting cases of Mie scattering is Rayleigh scattering, occurring when the size of the particle is much less than the wavelength – λ - of the light. A typical combustion gas molecule has a size much less than 1% of the wavelength of 500 nm light, and so meets this criterion.

Section 2.1.3 discussed Rayleigh scattering from particulate matter. While the fundamental scattering phenomenon is the same for molecular scattering as for small particles, the way in which it is used is quite different, being concentrated on gas density measurements rather than scatterer size determinations, and having very significant application to velocity measurements.

Because the Rayleigh-scattered light has the same wavelength as the incident light, viewing of the Rayleigh-scattered light must be done in a way which rejects the incident light, other elastically-scattered light of the same wavelength, and light adventitiously of the same wavelength, but generated by other, inelastic mechanisms.

Rejection of the incident light is the simplest, achieved by viewing the sampling volume at an angle to the incident light, so that only scattered light is seen. The next most important source of other scattering is scattering from finite-size particles, which, simply by virtue of their greater size, will scatter much more light than will the molecules. This normally necessitates that Rayleigh scattering, as discussed here, be done in flames with no particulates, making it primarily a research tool to be used in clean flames, rather than a diagnostic tool for practical burners. Reflections from walls, windows, etc. will, again, give spurious signals which must be calibrated out, usually in cold flow (Ref. 73, section 4a). This last calibration is not easy; Zhao (Ref. 74, par. 4.4.1) states that, because of this, free jets and open flames are the best suited for study by Rayleigh scattering.

2.3.2 Density Measurements

A review of the analysis in Eckbreth (Ref. 23, pp 209-213) shows that strictly elastic – that is, not Doppler shifted - Rayleigh scattering can only directly measure gas density, and only if the gas composition is known. Once the density is determined, the perfect gas law can be used to derive temperature. The need to know the gas composition is a complication in the use of Rayleigh scattering. This is addressed either by concurrently measuring the composition, by means which will be discussed in chapter 3, or by creating an experimental situation such that the composition can be inferred from calculations of the products of combustion. For some measurements, for which changes or fluctuations are of interest - as in turbulence - rather than absolute levels, the fact that combustible mixtures in air are about 75% nitrogen, which does not significantly react, can be used to justify treating the gas as having a constant composition (Ref. 74, p. 455). Notice that minority species can safely be ignored in calculating density.

While the scattering from an individual molecule can be written in terms of the wavelength and the polarizability and size of the molecule, a more useful formulation (Ref. 75, eqn. 11; Ref. 74,

eqn. 1) expresses the differential cross-section in terms of the number density – N_i - of the molecules and the index of refraction – n_i - of the pure gas at standard temperature and pressure (STP), and at a given wavelength - λ. Using Eckbreth's notation, the formula for the differential scattering cross-section of an individual scatterer to an angle Φ becomes:

$$\left(\frac{\partial\sigma}{\partial\Omega}\right)_{Ray,i} \cong \frac{4\pi^2}{\lambda^4}\left(\frac{n_i-1}{N_i}\right)^2 \sin^2\Phi\left(\frac{3}{3-\alpha_i}\right) \qquad (2\text{-}12)$$

By Avogadro's law, N_i is a constant, being $2.687\text{x}10^{25}$ m^{-3} in mks units. The term α_i arises from the anisotropy of the molecule; it quantifies the generation of a cross-polarization of the scattered wave relative to the incident wave, but, with a value that never exceeds 0.15, is normally taken to be zero. The scattering cross-section is only a weak function of temperature (Ref. 74, par. 2.2.1). With a mixture of gases, each with a mole fraction χ_i, the total differential scattering cross-section is the mole fraction-weighted sum of the individual scattering cross-sections:

$$\left(\frac{\partial\sigma}{\partial\Omega}\right)_{Ray,mix} = \sum_i \chi_i\left(\frac{\partial\sigma}{\partial\Omega}\right)_{Ray,i} \qquad (2\text{-}13)$$

Zhao (Ref. 74, par. 2.2.1) points out that the scattering cross-section can be viewed as the ratio of the scattered intensity to the incident irradiance.

Consider a detector viewing a laser-illuminated volume of length ℓ at an viewing angle $\Phi = \pi/2$, having total molecular density of N m^{-3}, with the viewing lens subtending a solid angle of Ω sr., and illuminated by a laser beam with a total beam power of P_{laser}. Then, once the Rayleigh scattered power P_{Ray} collected by the detector is measured, the number density of molecules, in principle, will be given by:

$$N = \frac{P_{Ray}}{P_{laser}\left(\frac{\partial\sigma}{\partial\Omega}\right)_{Ray,mix}\Omega\ell\varepsilon} \qquad (2\text{-}14)$$

where ε is the efficiency of the light collection and measuring system, and the formula assumes that the scattering from the full width of the beam is collected.

Once that this basic measurement of density is made, the addition of a pressure measurement allows the calculation of temperature. If the gas is a mixture of only two components, each with a known scattering cross-section, the addition of a separate temperature and pressure measurement allows determination of the mole ratios χ_i.

2.3.3 Doppler Effects

When referring to elastic scattering of light by a molecule, the scattering is elastic in the frame of reference of the molecule, which may result in a wavelength shift as viewed in a stationary frame of reference relative to which the molecule is moving. In particular, both random thermal

motion and a nonzero average motion relative to a stationary reference frame can give usable shifts of wavelength in the stationary reference frame.

Eckbreth (Ref. 23, p. 213) points out that, at atmospheric pressure, flame temperatures can be determined by fitting the observed scattered line shape to the Doppler frequency-broadened Maxwellian contour, using temperature as the fitting variable. Miles (Ref. 75, eqn. 58) gives the necessary equations and techniques, and states (Ref. 75, p. R45) that the Fabry-Perot etalon can be used for this measurement. The technique is only applicable at pressures such the density is below the level at which collisional broadening dominates. This condition is certainly satisfied for the atmospheric pressure free jet flames for which Rayleigh scattering is best suited. At the higher pressures at which practical devices are evaluated, an analysis which accounts for the collisional effects is necessary (Ref. 76, pp. 548-551). One seemingly potential problem for which I could find no discussion was how to distinguish between the broadening due to thermal motion and that due to turbulence; it may well be that, since thermal velocities are of the order of the speed of sound, while turbulent fluctuations are of considerably lower velocity, that turbulent fluctuations will not contribute significantly to the broadening.

One way of measuring the wavelength shift of the scattered light due to the mean velocity is by heterodyning it against the incident beam, as shown in the following diagram:

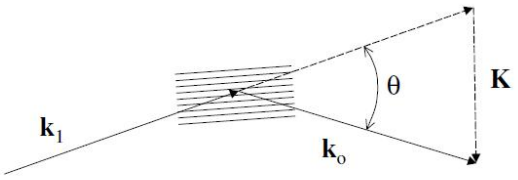

Figure 6. Scattering vector diagram. The incident wave vector is $\vec{k}_1$ and the scattered wave vector propagating to the observer is $\vec{k}_0$. These two vectors define an interference vector in the direction $\vec{K} = \vec{k}_0 - \vec{k}_1$ and an associated interference structure scale $\lambda_s = 2\pi/\vec{K}$.

Fig. 2.8 – Mixing of Incident and Rayleigh-Scattered Wave. (Ref. 75, fig. 6)
This diagram shows how the incident wave – k_1 - and the Rayleigh-scattered and Doppler-shifted wave – k_0 - can interfere to create a moving fringe pattern as viewed by the observer, which can be used for gas velocity measurements.

A molecule traveling with a speed u at an angle δ - in the plane common to k_1 and k_0 - relative to the difference vector K will give a scattered frequency of

$$f = \frac{2u}{\lambda}\cos(\delta)\sin(\frac{\theta}{2}) \qquad (2\text{-}15)$$

From measurements of f and knowing θ, $u \cdot cos(\delta)$ can be derived. While none of the references then address this point, it seems that, at any given location, a velocity determination necessitates variation of k_1 and k_0 until the maximum value of $u \cdot cos(\delta)$ results, implying that $\delta=0$ and that the absolute velocity and direction are now determined. The technique has a sensitivity comparable

to the particle scattering techniques described in chapter 4, suffering, however, from the fact that scattering from molecules is much weaker than is scattering from particles.

There is a similarity between equation 2.12 above, and equation 4.1. Physically, there is the difference that the interference being currently discussed is not between two fixed planar waves (as in Ch. 4), but between a planar incident wave and a non-planar scattered wave. Also, the angle θ is not set by the angle between two planar waves, but rather by the chosen angle of observation which determines k_θ.

This interferometric technique can have a good sensitivity for low flow velocities by measuring the beat frequency with an optoelectronic detector. This will "max out" when the frequency exceeds the capability of the frequency detector. At that point, an alternative approach which uses Fabry-Perot interferometry to determine the frequency shift of the scattered light from the incident light becomes practical. This technique is explained in detail in Ref. 76. In either event, the frequency shift measured by Doppler Rayleigh scattering will be the sum of the random thermal velocity, turbulent fluctuations, and the mean velocity. Consequently, the resultant measured velocity will actually be a spectrum, rather than a single value, with the turbulent fluctuations and the thermal agitation serving to broaden the line around the mean shift. The inherent limitations of the Fabry-Perot interferometer are such that it can only be used for velocities of the order of hundreds of meters per second. The analysis of section 4.1.1.5 is relevant here.

The technique can be expanded to a multiaxis measurement of velocity. Ref. 79 describes such a system.[1]

Speeds of hundreds of meters per second are characteristic of the Maxwellian thermal velocities of gas molecules. As mentioned before, the Maxwellian velocities will broaden the spectral line and this broadening can be used to determine the temperature from the Fabry-Perot spectrum (Refs. 77 & 78). Turbulent fluctuations are typically much less, and so will not significantly modify the Fabry-Perot spectrum. As shown in Refs. 77 & 78, the assumption of a simple Maxwellian velocity distribution is valid only at low densities, and must be corrected for collective effects at densities above normal atmospheric densities; ref. 78 develops this technique in detail.

Chapter 4 will delve more deeply into laser Doppler anemometry, which shares much in common with velocity measurements using Doppler-shifted Rayleigh scattering. The techniques discussed in ch. 4 involve scattering of light from finite-sized particles introduced into the flow, rather than from the molecules in the flow. Some advantages and disadvantages of each follow from these, as follows:

1) Scattering from particles entrained in the flow will be Doppler-shifted too, but will have scattering cross-sections orders of magnitude greater than individual molecules, thus giving a much stronger and easily-measured signal, but also swamping out the molecularly-scattered signal;

[1] Reference 79 is a real *tour de force* of optical design.

2) Finite-sized particles cannot perfectly follow the flow, leading to increasing errors as the flow accelerations increase. This problem becomes especially serious if the measurements are being made at pressures well below atmospheric, as is often necessary for flame structure and other specialized studies;
3) Molecules ARE the flow, so that the problem in (2) above does not exist when making velocity measurements from molecularly-scattered light.
4) The relatively large particles used in LDA do not respond to thermal agitation, so that the fluctuation due to turbulence can be measured.
5) The LDA technique can remove the ambiguity of positive and negative velocities giving the same beat frequency by frequency-shifting one of the beams; it would appear that this could be done with Rayleigh scattering by frequency shifting the scattered beam, but I have found no indication that this is being done.

3. INELASTIC SCATTERING PHENOMENA AND THEIR APPLICATION

3.1 BACKGROUND

Inelastic scattering phenomena are those in which the incident wave exchanges energy with the medium being measured, so that the scattered wave is at a different wavelength than is the incident wave. In the present context, the exchange of energy is with the internal energy modes of molecules – electronic, vibrational, and rotational. In this chapter, the term "molecule" can include individual atoms.

3.1.1 The Nature of Spectra

The quantization of energy levels in a molecule is such that, for the most part, the different modes of energy storage will absorb or emit in distinct wavelength bands. In an attempt to provide a unified description of these, we have the following approximate spectral characteristics of the emissions of different transitions:

Outer shell electronic transitions (visible and ultraviolet) –
wavelength – 100 nm to 1000 nm
energy – 12.4 ev. to 1.25 ev
frequency – 3 PHz to 300 GHz

Molecular vibrational transitions (infrared) -
wavelength – 700 nm to 100,000 nm (0.1 mm)
energy – 1.8 ev. to 0.012 ev
frequency – 432 GHz to 2.9 Ghz

Molecular rotational transitions (microwave) –
wavelength – 10^5 nm (0.1 mm) to 10^8 nm (10 cm)
energy – 1.2×10^{-2} ev. to 1.2×10^{-5} ev.
frequency – 2.9 GHz to 2.9 MHz

Inner shell transitions (giving rise to X-rays) are of limited significance in combustion and gas-dynamic measurements.

A transition between two energy levels will give a spectral line. Transitions between two other energy levels will give a line at a different wavelength. A group of transitions between related levels will create a "band" of lines, having similar wavelengths.

Typically, purely electronic and purely vibrational bands will have widely spaced lines at one extreme of the band, coalescing to a near continuum at the other end of the band. The wavelength spacing of the widely spaced lines is usually comparable to the wavelength of the lines themselves – typically 1/10 to ¼ of the wavelength.

Typically, purely rotational bands will tend to have a uniform spacing of lines, though these are much more closely spaced than are vibrational or electronic lines.

A given transition event can be a combination of two (or even three) modes – for instance, a transition from one vibrational state within a higher electronic state to a different vibrational state within a lower electronic state – or practically any other combination of state changes imaginable. Because the wavelengths for the different types of transitions within a given molecule are typically so different, the spectral lines corresponding to the simultaneous occurrence of two types of transitions (for instance, vibrational and rotational) will consist of widely-spaced lines of the higher-energy transition, with side lobes – or broadening – arising from the lower energy transition. For example, the spectra of simultaneous transitions between rotational and vibrational states will consist of widely-spaced lines corresponding to the vibrational transitions, each vibrational line accompanied by a cluster of closely-spaced lines corresponding to the rotational transitions.

Further, due to coupling between modes of energy storage, the energy levels and the associated energy level changes of one mode can be altered by the absolute levels of another. To give a specific case, the changes in moment of inertia associated with different vibrational amplitudes causes the angular momentum, and the associated rotational energy, of a rotational state to change energy when the vibrational state changes. Thus, purely vibrational changes will have multiple possible changes of energy due to the different rotational energy changes. The bad news is that this means that vibrational energy lines will be broken up into a closely-spaced group due to the associated rotational changes. The good news is that these groupings allow rotational spectroscopy of a very refined sort.

A similar effect occurs with simultaneous electronic and vibrational transitions – widely spaced lines of the electronic transitions are accompanied by more closely-spaced lines of vibrational transitions.

There are additional refinements due to such things as nuclear spin, etc. However, these are not directly significant for the determination of molecular properties and states.

3.1.2 The Relevant Phenomena

Because fluid dynamic and combustion investigations must, of necessity, resolve the effects of rapid spatial changes, spatial precision is a necessity. Eckbreth (Ref. 23, p. 35) names four primary spatially precise techniques for temperature and species measurement. Two are incoherent – that is, they scatter light throughout 4π steradians, but not necessarily isotropically, and are not particularly synchronized with the incident beam. Two are coherent – that is, the data is carried on a focused beam which is created synchronously with the incident beam.

The incoherent techniques are Raman scattering and laser induced fluorescence. The coherent techniques are coherent anti-Stokes Raman scattering and degenerate four wave mixing. The "Physical Bases" section of this report will describe the underlying mechanisms of these four techniques, and the "Application" section will describe how they are used.

3.2 PHYSICAL BASES

3.2.1 Incoherent Technique - Laser-Induced Fluorescence

Laser-induced fluorescence (LIF) involves the excitation of electronic states of the molecule, much in the same way as are molecules in a visible wavelength laser.[2] Indeed, many of the parameters used to analyze pumping of a lasing medium – the Einstein B coefficient, fluorescence lifetime (related to the Einstein A coefficient), collisional quenching, and pressure broadening - are also relevant to the analysis of LIF spectra. While LIF was just stated to involve electronic excitation and decay, each electronic energy level can contain a multiplicity of vibrational and rotational levels, so that an "electronic" transition can involve a transition between vibrational and rotational levels as well. Fig. 3.1 gives a schematic of these changes.

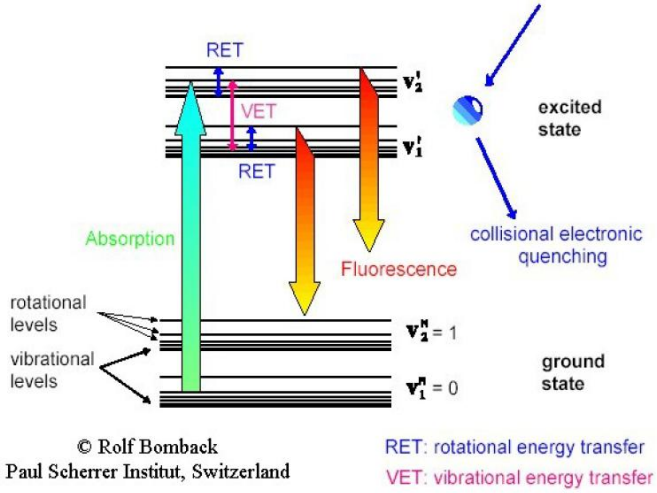

Fig. 3.1 – Schematic of Energy Level Transitions Used in LIF
(Ref. 58, Fig. 1.1)
This figure illustrates the energy transitions giving absorption and fluorescence in LIF. We see that the greater energy transitions, and so the shortest wavelengths, are between the electronic levels, which yields light typically in the visible range. However, we also see that each electronic energy level is modified by multiple vibrational and rotational energy levels, which modulate the frequency/wavelength of the emitted/absorbed visible light by an amount which is characteristic of the vibrational and/or rotational spectrum of the molecule.

Further, while the excitation can initially be of a single electronic transition and a single vibrational transition, there can be transfer of energy between the vibrational states of the excited electronic states before the decay occurs (Ref. 25, p. 149, "stepwise line fluorescence"). These "vibrational smearing" effects appear as a cluster of closely-spaced vibrational lines between the

[2] While excitation of purely vibrational modes can be envisioned, this suffers from problems of interference, unavailability of tunable lasers in the wavelengths of interest, and inapplicability to homonuclear molecules.

more widely-spaced electronic lines. A similar effect arises with transitions between rotational states, shown as rotational lines between the vibrational lines, per Fig. 3.2 following.

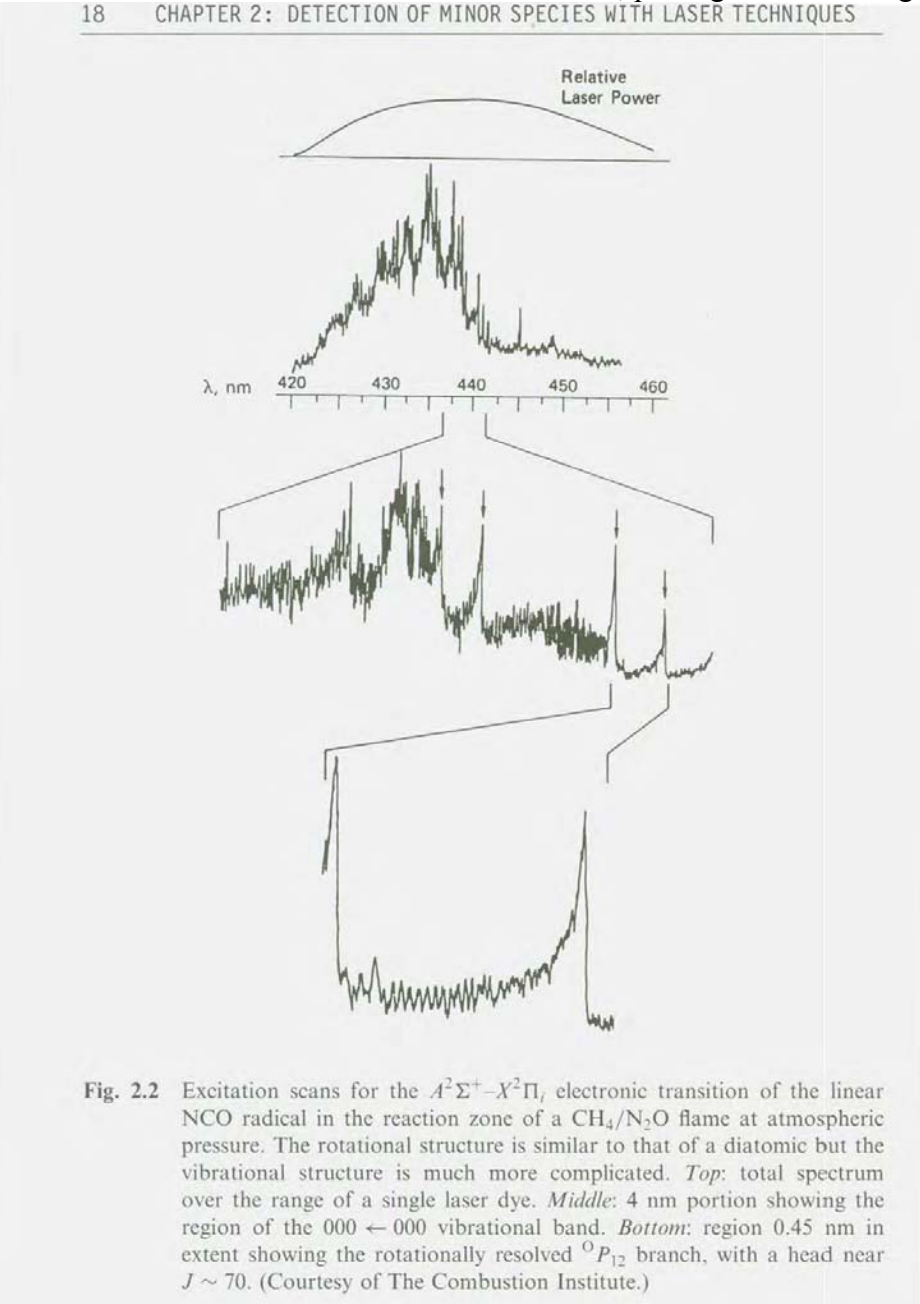

Fig. 3.2 – Detailed Example of Energy Level Transitions (from Ref. 24, Fig. 2.2)

This figure illustrates the segmentation of an absorption or fluorescence spectrum into higher and higher resolution segments, going from the visible band corresponding to electronic transitions to microwave-scale modulations corresponding to the rotational transitions. The top line is the spectrum of the laser excitation. The second line is the spectrum of the electronic states, which, in this case, is over the range of 420-460 nm, or about 0.7 PHz – clearly in the visible. The third line show a 4 nm bandwidth vibrational modulation of the spectrum,

corresponding to about a 6 GHz infrared modulation – indeed typical of a vibrational spectrum. The fourth line shows the 0.45 nm rotational modulation of the spectrum, corresponding to about a 700 MHz microwave modulation – typical of a rotational spectrum.

The relative probability of excitation of vibrational states is governed by the Frank-Condon principle, which depends on the overlap integral of the vibrational waveforms of the initial and of the final states, within the respective electronic states.

A LIF spectrum can be measured either as a fluorescence spectrum or as an excitation spectrum, with the difference illustrated in Fig. 3.3. The differences between the two are these: 1) A fluorescence spectrum is created by exciting the molecule with a specific laser wavelength, and measuring the multiple wavelengths of the spectrum of the subsequent emission, while; 2) An excitation spectrum is taken by recording the broadband emission resulting from scanning through multiple excitation wavelengths – the spectrum is taken of the excitation rather of the emission.

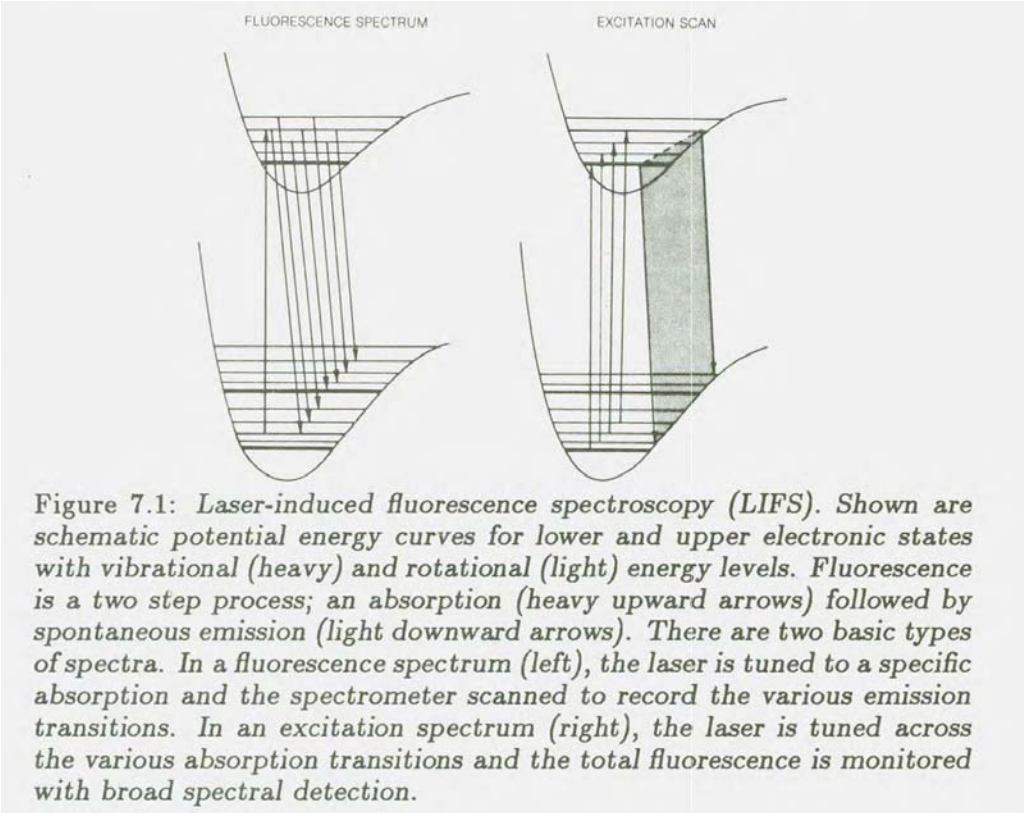

Figure 7.1: *Laser-induced fluorescence spectroscopy (LIFS). Shown are schematic potential energy curves for lower and upper electronic states with vibrational (heavy) and rotational (light) energy levels. Fluorescence is a two step process; an absorption (heavy upward arrows) followed by spontaneous emission (light downward arrows). There are two basic types of spectra. In a fluorescence spectrum (left), the laser is tuned to a specific absorption and the spectrometer scanned to record the various emission transitions. In an excitation spectrum (right), the laser is tuned across the various absorption transitions and the total fluorescence is monitored with broad spectral detection.*

Fig. 3.3 – Fluorescence vs. Excitation Spectra
(Ref. 23, Fig. 7.1)
This figure illustrates the difference between a fluorescence spectrum (left image) and an excitation spectrum (right image). The fluorescence spectrum is taken by creating a single excited state with a single exciting wavelength, and seeing the emission spectra of transitions; the excitation spectrum gets the same lines in absorption by scanning excitation over a range of possible transitions and seeing which are important by observing to total emission from the decay of each excitation.

Usually excitation is by a single photon process, which typically works down to excitation wavelengths of about 200 nm. However, below about 250 nm, gas phase absorption of the laser beam is very high, and single photon excitation no longer workable. The very high gas absorption of the shorter, "vacuum ultraviolet" wavelengths of less than 250 nm is circumvented by two-photon processes, achieved by pumping with a very intense beam of wavelength longer than 250 nm, such that two photons can be absorbed at a time, and the rate of pumping is proportional to the square of the laser irradiance instead of linearly. There is the problem that the two-photon cross-section is much smaller than is the single photon cross-section.

Because LIF excitation is tuned to specific absorption lines of the molecules of interest, it is inherently very sensitive, and suitable to the detection of very low concentrations. The down side here is that the major features of the electronic and vibrational spectrum of the specific species must be known *a priori*.

The picture is complicated, but not changed, by the fact that there are significant non-radiative transitions as well as radiative transitions. This will be discussed in section 3.3.2.1 – "Species Measurement by LIF".

3.2.2 Incoherent Technique - Spontaneous Raman Scattering

A radio engineer would describe spontaneous Raman scattering as a heterodyning procedure, in which a wave of one frequency, incident on a circuit (molecule) with a different (and much lower) resonant frequency, will have some scattering at side lobe frequencies which are the difference and the sum of the incident frequency and the resonant frequency. If the resonant frequency is replaced by a spectrum of frequencies, the side lobes are replaced with replicas of the original spectrum, but with frequencies in the range of the incident wave rather than of the original, much lower resonant frequencies. Continuing the interchange between radio and spectral terminology, the main lobe, corresponding to the carrier frequency, is the elastically scattered Rayleigh signal.

Figs. 3.4 and 3.5 give simplified examples of representative Raman spectra. In both cases, we see a central peak – the "Rayleigh line" - corresponding to the unaltered incident frequency, which is independent of the molecular character. In both cases, side lobes are excited whose shape and position relative to the exciting frequency are characteristic of the particular molecule. Fig. 3.4 makes this particularly clear, showing that, whether the exciting frequency is near IR or is visible, the Raman side lobes are located in the same position relative to the main lobe.

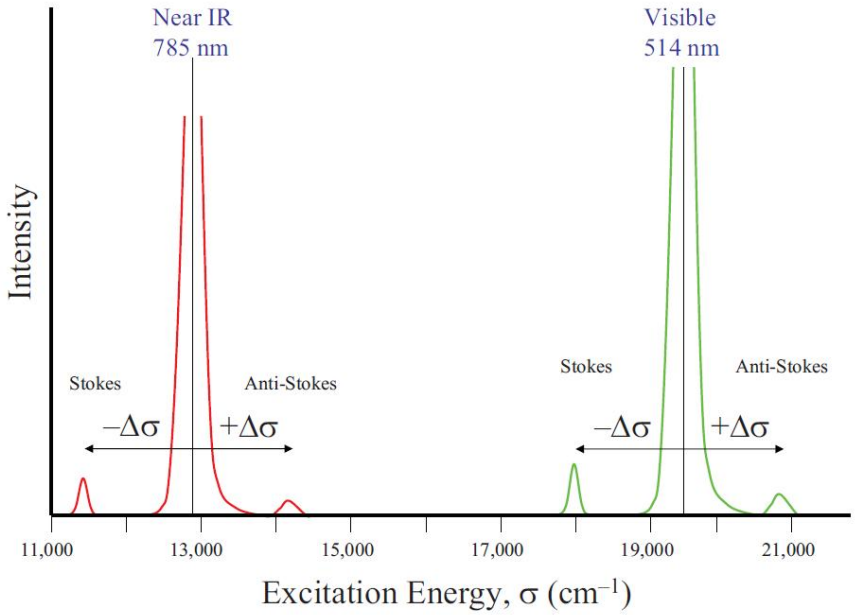

Fig. 3.4 – Raman Side Lobes (Ref. 59, slide 7)
This illustrates that, in Raman scattering, the frequency offset of the Stokes and anti-Stokes lobes from the exciting frequency is a constant, dependent only on the molecular character and independent of the exciting frequency.

We can also see that, because rotational energy increments are so much smaller than are the vibrational energy increments, the rotational energy spectra serve to broaden the vibrational bands. In the case of what is called the "Q band" of no vibrational changes, the rotational energy spectra provide a broadened base around the carrier frequency. Of course, higher resolution spectroscopy would resolve the rotational peaks within the vibrational band. Fig. 3.5 more clearly shows the relative frequency changes of the vibrational and rotational bands. Both Figs. 3.4 and 3.5 show that the higher frequency anti-Stokes wing is weaker than the lower frequency Stokes wing, exactly as would be expected from statistical mechanics.

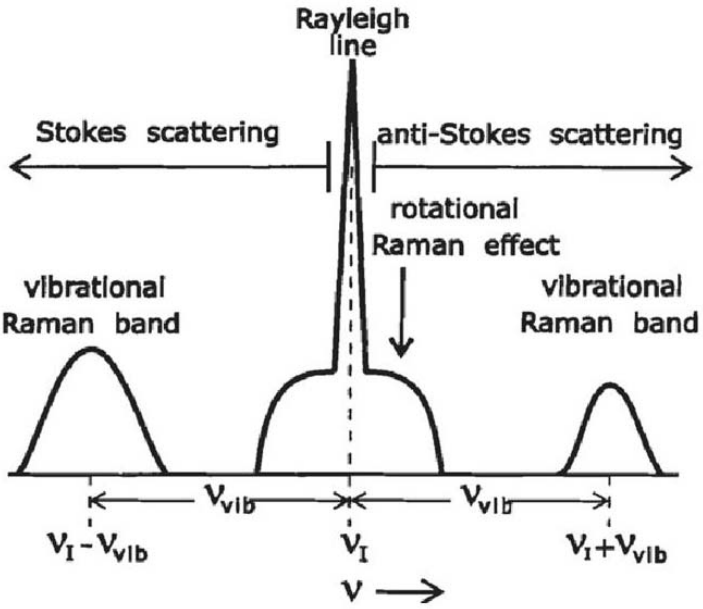

Fig. 3.5 – Rayleigh Line, and Raman Broadening and Side Lobes (Ref. 26, Fig. 8.2). This again illustrates that the Stokes and anti-Stokes wings arising from vibrational modes will be offset by a constant amount from the exciting frequency, and that all three lobes are broadened by the rotational modes.

Qualitatively, we can use quantum mechanics to visualize how this happens. Each line of the original spectrum corresponds to a vibrational or rotational level change of the original molecule. If it is excited by the incident beam, it will steal a corresponding amount of energy from the incident beam, causing the beam's frequency to be shifted downward by the corresponding amount. In the event that the excitation is already active, it can - much less frequently - give up its energy to the incident wave, so shifting its frequency upward. The original spectrum is now replicated as a shorter wavelength side lobe of the incident wave. The longer wavelength sidelobe is called the "Stokes" lobe; the shorter wavelength side lobe is called the "anti-Stokes" lobe.[3]

There is also coherent Raman scattering which will be discussed in the next section – it gives the same wavelength-shifted spectrum, but by a slightly different – though related - nonlinear polarization process.

Why bother? Most superficially, Raman scattering shifts infrared or microwave spectra into the optical range, making them analyzable by the powerful techniques of optical spectroscopy. But in addition, by quantum mechanics, some vibrational modes will not be excited directly by resonant infrared radiation because of the symmetry of the molecule and the corresponding lack of a dipole moment. These modes can, however, be excited by much higher frequencies due to nonlinearity of the polarizability of the molecule, rather than its polarizability itself (Ref. 23, p. 218). Thus, Raman spectra will include vibrational lines which are invisible in infrared spectra.

[3] The description is qualitative because the actual mechanism of generation of the side lobe frequency arises from a nonlinearity of the molecular polarizability – see eqn. 5.16, Ref. 23.

3.2.3 Coherent Technique - Coherent Raman Spectroscopy

Coherent Raman spectroscopy is a technique in which two waves of different frequency are mixed by interacting in a nonlinear medium to produce a third wave. What is unique about the procedure is that the difference between the frequencies, when it matches a vibrational or rotational frequency of the medium, is amplified in a coherent beam with the spectral characteristics of the vibrational or rotational spectrum. Thus, we get the same spectrum as in incoherent Raman scattering, but with much more intensity. Normally, the anti-Stokes wing of the spectrum is chosen (for reasons that will be explained shortly), so the usual reference is to coherent anti-Stokes Raman spectroscopy (CARS).

To understand how CARS works, we begin with the nonlinear susceptibility, relating polarization - $\vec{P}$ - to the applied electric field - $\vec{E}$:

$$\vec{P} = \vec{E}\left[\chi^{(1)} + \left|\vec{E}\right|\chi^{(2)} + \left|\vec{E}\right|^2 \chi^{(3)}\right]\varepsilon_0 \qquad (3\text{-}1)$$

The first order term will simply give a replica of whatever field is applied, perhaps with a change of amplitude and a phase shift.

Tolles (Ref. 27, p. 254) argues that the second order term – $\chi^{(2)}$ – must be zero in an isotropic medium such as a liquid or a gas, in contrast to the situation in a solid, whose anisotropy permits a second order term.[4] Consequently, the first nonlinearity in a gas or liquid arises from the third order term - $\chi^{(3)}$, and this third order term is the one of interest here.

Consider exciting the gas with an E field which is the sum of two terms of different frequencies

$$\left|\vec{E}\right| = a\sin(\varpi_1 t) + b\sin(\varpi_2 t) \qquad (3\text{-}2)$$

where, for simplicity, the E and P fields will now be treated as scalars. Then the response of the first-order term will be

$$\left|\vec{P}\right|^{(1)} = \chi^{(1)}[a\sin(\varpi_1 \mathrm{t}) + b\sin(\varpi_2 t)]\varepsilon_0 \qquad (3\text{-}3)$$

This is simply a pair of waves with the original frequencies, modified in amplitude and phase. The response of the third order term will be

$$\left|\vec{P}\right|^{(3)} = \chi^{(3)}[a\sin(\varpi_1 t) + b\sin(\varpi_2 t)]^3 \varepsilon_0 \qquad (3\text{-}4)$$

The expression in brackets can be expanded, by the binomial theorem, as

$$\sum_{l=0}^{3}\left(\frac{3!}{l!(3-l)!}\right)[a\sin(\varpi_1 t)]^{(3-l)}[b\sin(\varpi_2 t)]^l \qquad (3\text{-}5)$$

[4] It is the second order term in a solid which permits frequency doubling in Nd:YAG lasers.

The next matter of interest is to determine the frequencies which result from this nonlinear mixing procedure. This will be developed in some detail, as this development is absent from any of the references I found. For this development, the exact value of the coefficients can be ignored, and be replaced by the dummy value *d*. First of all, consider the cases $l = 0, 3$. For these two cases, the term is

$$d\sin^3(\varpi t)$$

where ω is ω_1 for $l = 0$, and ω_2 for $l = 3$. This can be expanded as

$$\frac{d}{4}[-\sin(3\varpi t)+3\sin(\varpi t)]$$

Thus, one result of the mixing process is that a weak third harmonic and a slightly weakened first harmonic are generated for each of the two input frequencies.

The matter of central interest for CARS, however, are the terms for $l = 1,2$. These terms have the form

$$d\sin^2(\varpi_a t)\sin(\varpi_b t)$$

For $l = 1$, the subscripts (*a*) = *(1)* and (*b*) = *(2)*; and for $l = 2$, *(a) = (2)* and *(b) = (1)*. A further expansion by trigonometric identities gives

$$\frac{d}{2}[-\cos(2\varpi_a t)\sin(\varpi_b t)+\sin(\varpi_b t)]$$

The product term can be further expanded by the trigonometric identity

$$\sin(a)\cos(b)=\frac{1}{2}[\sin(a+b)+\sin(a-b)] \qquad (3\text{-}6)$$

to yield the final form

$$\frac{d}{2}\{\sin(\varpi_b t)+\frac{1}{2}[\sin(\{\varpi_a+\varpi_a-\varpi_b\}t)-\sin(\{2\varpi_a+\varpi_b\}t)]\}$$

Thus, we see that for <u>each</u> of the two input frequencies, a total of four output frequencies have been generated – the base frequency equal to the input frequency, a third harmonic of the input frequency, and two beat frequencies. Now per Tolles, (Ref. 27, p. 254) the component of interest for CARS is the component

$$\sin[\{\varpi_a+(\varpi_a-\varpi_b)\}t]$$

which has been re-written to show that it is an upper side lobe of the frequency ω_a. We see immediately that the spectral location of the side lobe can be adjusted by adjusting the frequency ω_b.

We now proceed to connect this with existing analyses of CARS, and adopt the terminology of Regnier & Tarnan in Ref. 26, p. 87. The beam of fixed frequency - $\omega_{\mathbf{a}}$ – will be the "laser" – $\omega_{\mathbf{l}}$. The adjustable frequency – $\omega_{\mathbf{b}}$ - will be called - and shown to be - the "Stokes" frequency – $\omega_{\mathbf{s}}$. The resultant frequency on the high side $\omega_{\mathbf{a}} + (\omega_{\mathbf{a}} - \omega_{\mathbf{b}}) \equiv 2\omega_{\mathbf{l}} - \omega_{\mathbf{s}}$ – will be called the "anti-Stokes" frequency - $\omega_{\mathbf{as}}$.= The lower side lobe "Stokes" frequency will be symmetrically at $\omega_{\mathbf{a}} - (\omega_{\mathbf{a}} - \omega_{\mathrm{b}}) = \omega_{\mathbf{b}} \equiv \omega_{\mathbf{s}}$, which is why it is called the "Stokes" frequency.

We now have generated an anti-Stokes frequency, but implicitly only at one point. It is of no use unless it can be propagated to instruments and measured. Thus, we must next demonstrate that it will propagate separately from the two generating waves, separately subject to its own spectral analysis. We first engage in a bit of qualitative thinking. When we add two waves, we get the maximum effect when peaks align with peaks, and valleys align with valleys. But if two waves have different wavelengths, this alignment cannot persist if they are collinear – they will drift in and out of phase, and never build up a significant amplitude. The problem can be solved by angling the shorter wavelength wave with respect to the longer wavelength wave, so that the projection of the shorter wavelength on the longer wavelength direction of propagation exactly equals the longer wavelength. Of course, the resultant (anti-Stokes) summation wave will go in yet a third direction, but this is an advantage because it allows spatial filtering to be used to reduce background.

Using the same subscript notation as for frequencies, Regnier and Tarnan define a parameter

$$\Delta\vec{k} = 2\vec{k_l} - \vec{k_s} - \vec{k_{as}} \qquad (3\text{-}7)$$

which they call the "momentum mismatch". As the anti-Stokes wave propagates, they show that the growth with distance – L – along a direction – z - is proportional to

$$\left| \int_0^L dz * \chi(\varpi_{as}) e^{iz\vec{\Delta k}} \right|^2$$

We notice that: 1) If the momentum mismatch $\vec{\Delta k}$ is <u>not</u> zero, the integrand will be a sinusoid and the anti-Stokes beam will not grow; 2) If the susceptibility – χ - is significant at a particular anti-Stokes frequency, the beam will grow at that frequency, and; 3) If the momentum mismatch <u>is</u> zero, then the signal will grow quadratically with distance - L. The growth in the magnitude at ω_{as} of items (2) and (3) comes from photons scattered in from $\omega_{\mathbf{l}}$ and $\omega_{\mathbf{s}}$. The susceptibility of item (2) can be associated with any of electronic, vibrational, or rotational modes of the molecule, and so serves to create a spectrum.

Given a refractive index $n(\omega)$ and a frequency ω, the absolute value of the associated wave vector becomes

$$\left|\vec{k}\right| = \frac{\varpi \bullet n(\varpi)}{c} \qquad (3\text{-}8)$$

where c is the speed of light in vacuum.

Then the momentum matching condition becomes:

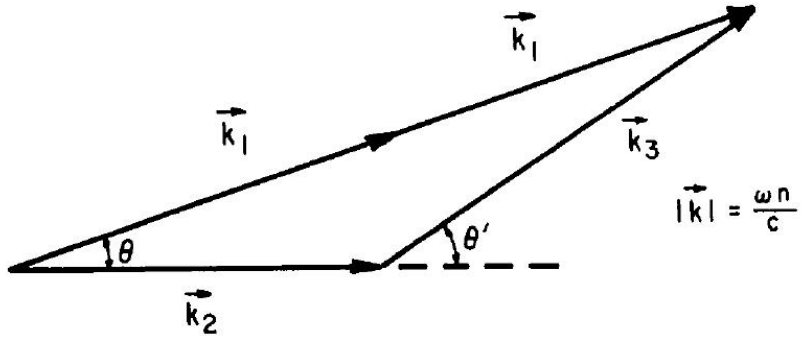

$$2\omega_1 - \omega_2 = \omega_3$$

Fig. 3.6 – Momentum Matching of Two Different Wavelengths
$\left(\textit{Fig. 2 of Ref. 27, with } \vec{k}_l \to \vec{k}_1; \vec{k}_s \to \vec{k}_2; \vec{k}_{as} \to \vec{k}_3\right)$

This illustrates how two waves of different wavelengths can be added to yield a third wave, provided that the directions of the three waves of interest are not collinear.

This is a simple problem in trigonometry, which is solved by successive application of the law of cosines

$$\theta = \cos^{-1}\left[\frac{\left|2\vec{k}_l\right|^2 + \left|\vec{k}_s\right|^2 - \left|\vec{k}_{as}\right|^2}{2\left|\vec{k}_l\right|\left|\vec{k}_s\right|}\right] \approx \cos^{-1}\left[\frac{(2\omega_l)^2 + (\omega_s)^2 - (\omega_{as})^2}{2(\omega_l)(\omega_s)}\right] \qquad (3\text{-}9)$$

and the law of sines

$$\theta' = \sin^{-1}\left(\frac{2\left|\vec{k}_l\right|}{\left|\vec{k}_{as}\right|}\sin(\theta)\right) \approx \sin^{-1}\left(\frac{2(\omega_l)}{(\omega_{as})}\sin(\theta)\right) \qquad (3\text{-}10)$$

The relations involving frequencies are approximations if the material is dispersive – if the indices of refraction are the same for the three frequencies, the approximation becomes an equality.

Thus far, the following has been shown: By combining two intense beams of slightly different frequency in a material with a cubic component of susceptibility, at a carefully chosen angle, a third, coherent beam has been generated which can be Raman active on the high frequency side of either of the two exciting beams, and so is anti-Stokes. Thus, we do indeed have a coherent, anti-Stokes Raman spectrum. Because of the coherence and the intensity of the excitation, the laser-like beam carrying the spectrum has a considerably greater irradiance than does an incoherently scattered Raman spectrum.

The Stokes beam is not used because it contains a very large component from the linear portion of the susceptibility, which will not be modulated by nonlinearities to yield a Raman spectrum.

3.2.4 Coherent Technique –Four Wave Mixing (Degenerate and Resonant)

Degenerate four wave mixing (DFWM), like CARS, also operates by virtue of the cubic term of the nonlinear susceptibility of an isotropic medium. Recapitulating, the coefficient of this cubic term depends on frequency, being particularly enhanced when it corresponds to an internal transition of a molecule. Plotting the wavelengths of these internal transitions is what yields the spectrum of the molecule – its "fingerprint". Implicit to all of this is the availability of tunable lasers. While the excitation is primarily from a lower electronic state to a higher electronic state, the concurrent occurrence of changes of vibrational and of rotational states means that vibrational and rotational spectra occur as side lobes of the electronic spectral lines.

In the preceding discussion of CARS, the tuning was used to generate a difference frequency which carried the signal, and which could be picked off by sensing it at the correct angle.

In DFWM, everything is at a single frequency – a single laser provides all of the beams, so that all of the beams' frequencies change together as the source laser's frequency is swept.

While the CARS tuning to resonant modes of the medium works by the difference of the two exciting beams exciting a resonant frequency of the medium, DFWM works by the exciting beam itself tuned to such a frequency – usually an electronic transition. Notice that, unlike LIF, there is no need for *a priori* knowledge of the resonant frequency.

3.2.4.1 Description of DFWM

DFWM can be described and analyzed by two paradigms – called here the Bragg reflector model and the nonlinear coupling model. The Bragg reflector model is the easier to visualize (Ref. 35), while the nonlinear coupling model provides quantitative results.

3.2.4.2 Bragg Reflector Model

Fig. 3.7 following, taken from Ref. 28, depicts DFWM.

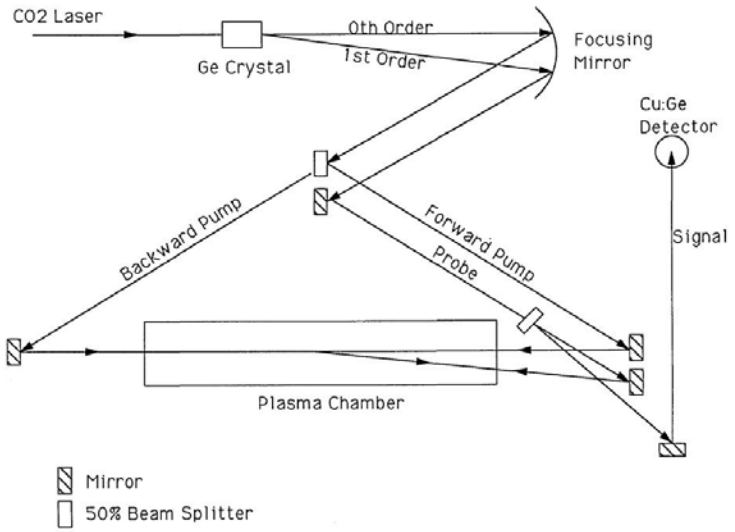

Fig. 3.7 – Schematic of Degenerate Four-Wave Mixing (Ref. 28, Fig. 1)
The beam is separated at the germanium crystal into two components – a pump beam (0-th order) and a probe beam (1st order). The pump beam is then further split into equal forward and backward pump beams by the first beam splitter, which two pump beams then interact nonlinearly in the chamber to create a Bragg grating. At the same time, the probe beam, introduced into the chamber at a slight angle, is reflected by the Bragg grating, ultimately being measured by the Cu:Ge detector.

The DFWM itself occurs in the "plasma chamber", though in the present discussion it is a volume of gas rather than a plasma. The forward and the backward pump beams interfere to form a standing wave pattern. Normally, the presence of the standing wave would have no effect on the optical properties of the material in the gas. However, if the E field of the pump beams is very large, the nonlinear susceptibility becomes manifest, giving variations of refractive index – n - in accordance with the relationship:

$$n = \left(1 + \chi^{(1)}(\varpi) + \chi^{(3)}(\varpi) \cdot \left|\vec{E}\right|^2\right)^{1/2} \qquad (3\text{-}11)$$

The usual case is that

$$\chi^{(3)}(\varpi) \cdot \left|\vec{E}\right|^2 \ll \left(1 + \chi^{(1)}(\varpi)\right) \qquad (3\text{-}12)$$

so that the CHANGE of refractive index as E goes from $0 \rightarrow E$ can be written, after applying the binomial theorem, as

$$|\Delta n| = \frac{1}{8} \frac{\chi^{(3)}(\varpi)\left|\vec{E}\right|^2}{\left[1+\chi^{(1)}(\varpi)\right]^{1/2}} \qquad (3\text{-}13)$$

In addition, the usual case for gases is:

$$\chi^{(1)}(\varpi) \ll 1 \qquad (3\text{-}14)$$

so that

$$|\Delta n| = \frac{1}{8}\chi^{(3)}(\varpi)\left|\vec{E}\right|^2 \qquad (3\text{-}15)$$

The E field in the standing wave interference pattern of the two pump beams will be given by the formula:

$$\sin(\varpi t)\cos(\vec{k}\cdot\vec{r})$$

The index of refraction changes with the square of the E field, so this variation of index of refraction induced by the interference pattern will create a Bragg reflector with a wavelength of ½ the wavelength of the pump beams. The probe beam, of the same wavelength as the pump beam, is intended to reflect from this Bragg reflector. In this case, the Bragg formula for reflection from plane, parallel, and implicitly infinite layers becomes:

$$d\lambda = 2\frac{\lambda}{2}\sin(\theta) \qquad (3\text{-}16)$$

d here is the order of the reflection, which is a positive integer. The only possible solution is $\theta = 90°$ - the probe beam, ideally, should be parallel to the pump beams. Because the interference pattern is intentionally created in a small cross-sectional area, the probe beam can be moderately off-axis (a value of 3º is cited in Ref. 28) and still be reflected, which is desirable because the intent is to create a small interaction volume for localized probing of the gas.

Recapitulating, the Bragg reflector model explains DFWM as follows: The pattern of pump and probe beams is established, with the pump beams creating an induced Bragg reflector. The reflection of the probe beam from the induced Bragg reflector – called the "signal" beam – varies with the change of index of refraction induced by the nonlinear portion. The greater the change of index of refraction, the greater the magnitude of the reflected signal beam. But as the frequency of the beams is changed, the third order susceptibility also changes as different internal modes of molecules are excited. With this, a spectrum can be obtained.

3.2.4.3 Nonlinear Coupling Model

This approach involves quantum mechanics. It is harder to understand, but gives quantitative rather than qualitative results. The physical model developed is this: The excitation created by the powerful pump beams will have a component in which molecules are promoted out of lower energy states to higher energy states, as is usually the case with pumping. In addition, the excitation will also have a component in which induced molecular polarizations will be aligned

on a large scale. This is the nonlinear polarizability. The decay of the respective stored energies means that a probe beam will have a backscattered signal beam which grows – laser-like - with distance. Refs. 29 & 30 are the basic references of this phenomenon. They model the probe and the signal beams as interacting with each other and with the environment created by the pump beams, yielding mathematical relations for the growth of the reflected beam which are quite incomprehensible. The results are cast into a comprehensible form in Ref. 31. The coefficients of this interaction depend on the irradiance of the pump beams, various properties of the molecule, the density of the gas, the rate of collisional de-excitation of excited states, and, most importantly for spectroscopy, on the detuning of the pump beams from the line center of any adjacent spectral line. Again, the spectrum is obtained by sweeping the frequency of the beams, and detecting spectral lines by an enhancement of the signal beam when the frequency matches the spectral line.

The fact that the induced excitation has two components means that there will be two characteristic times for decay of this excitation – the "longitudinal" relaxation time T_1, and the "transverse" relaxation time – T_2. The terms "longitudinal" and "transverse" should be viewed as abstractions – they refer, not to physical directions, but to on-diagonal and off-diagonal terms of a quantum-mechanical matrix representation of the polarization. Physically, the "longitudinal" relaxation time is the familiar characteristic time for decay from a higher energy state to a lower energy state (ideally, the reciprocal of the Einstein A coefficient), and the "transverse" relaxation time is the characteristic time for the decay of the induced bulk polarization (Ref. 32). These relaxation times are dominantly collision-driven.

In turn, Ref. 32, pp. 72-73 reduces all this to the practical applications as follows: Using the notation of Ref. 32, a "saturation" irradiance can be defined at the center of a spectral line:

$$I_s(0) = \frac{h^2}{T_1 T_2 \left|\mu_{12}\right|^2} \qquad (3\text{-}17)$$

where h is Planck's constant, and μ_{12} is the dipole transition moment between states 1 and 2. A signal beam, which is the signal beam integrated over the spectral line width, is to be measured. For a pump irradiance much less than the saturation irradiance, this signal beam becomes:

$$I_{signal} \propto \left(\frac{\left|\mu_{12}\right|^8 N^2 T_1^2 T_2^3}{\left[1 + 4^{I_{pump}/I_s(0)}\right]^{5/2}} I_{pump}^2 \right) I_{probe} \qquad (3\text{-}18)$$

For a pump irradiance much greater than the saturation irradiance, the signal beam becomes:

$$I_{signal} \propto \left(\left| \mu_{12} \right|^3 N^2 \left[\frac{T_2}{T_1} \right]^{1/2} I_{pump}^{-1/2} \right) I_{probe} \qquad (3\text{-}19)$$

T_1 and T_2 are not too well known, and the dipole transition moment also has some uncertainty. However, there is an argument (Ref. 32) that T_1 and T_2 have a nearly fixed ratio. It is immediately obvious that the strong pumping case is much less sensitive to these uncertainties than is the weak pumping case. Thus, operating with strong pumping is normally preferred.

In both cases the signal is proportional to the square of N – very nearly the number of molecules per unit volume in the ground state of the transition 1→2, giving a good sensitivity at relatively low concentrations. More strictly, per Ref. 33, p. 153, N is actually the difference in the number of molecules between states 1 & 2 when there is no excitation. In most cases of interest here, the upper state is negligibly occupied when there is no excitation.

Because it is a laser-like pumping action which generates the signal beam, the signal beam is strong, coherent, and highly directional. The shortcoming is that, since it is at the same wavelength as the pump beams, background scattering can overwhelm the signal.

3.3 APPLICATIONS

Having given the physics, we will consider the application of these techniques to the two most important parameters in combustion – temperature and species concentration.

3.3.1 Temperature Measurements

Measurement of temperature by these means relies, in one form or another, on the Boltzmann relationship for the occupation of a state – j – having an energy ε_j and a "degeneracy" g_j – the degeneracy being the number of indistinguishable configurations which have the same energy. For instance, if the energy mode is kinetic energy ½mv^2, then the degeneracy is the number of possible combinations of the three components of the velocity which can have the same kinetic energy. Then, at a temperature T, the actual number of occurrences of that state – N_i - will be

$$N_i \sim g_i e^{-\frac{\varepsilon_i}{k_B T}} \qquad (3\text{-}20)$$

where k_B is the Boltzmann constant, whose exact value need not concern us at the moment. It then follows that, if we can get the ratio of the occupation of two states – p and q - of different energies, the temperature will be given by

$$T = \frac{\left(\varepsilon_q - \varepsilon_p\right)/k_B}{\ln\left(\frac{g_q N_p}{g_p N_q}\right)} \qquad (3\text{-}21)$$

Thus, temperature determination becomes a matter of determining the relative population of different energy states N_p, N_q, given that the g's have been determined in some way.

Because the transitions between levels of each of the various modes of energy storage have such different energy magnitudes, it is possible to separately identify transitions between vibrational, between rotational, and between electronic states. Translational energy determination is done somewhat differently, which will be discussed later. In particular, it turns out that the vibrational and rotational modes of energy storage are of most value in combustion measurements.

If we consider a ground state made of a vibrational state – v – and a rotational state – J – both within the same electronic level, then we will have an additional energy – $E(v,J)$ - made up of a vibrational part – $G(v)$ – and a rotational part – $F_v(J)$.

$$E(v,J) = G(v) + F_v(J) \qquad (3\text{-}22)$$

The functional form of F depends on v because changes in vibrational excitation cause changes in moment of inertia, which is a very important part of this technique. Also, the total degeneracy can be broken into the product of the nuclear spin degeneracy – g_J and the rotational degeneracy – $2J+1$ – with vibrational degeneracy normally being fixed at 1 for simple molecules, and the nuclear spin degeneracy changing with J (Ref. 34). Finally, "selection rules" for permitted transitions between various modes strongly limit the changes of v to either 0 or ± 1 quantum number, and the changes of J to 0 or ± 2 quantum numbers.

Consider a light scattering setup in which a laser beam of irradiance E_L is scattered to one side, and the scattered light is collected by an optical system. Then the power collected by the optical system – Φ – will follow the relationship

$$\frac{\Phi}{E_L} \sim \left(\frac{\partial\sigma}{\partial\Omega}\right) N_{vJ} \qquad (3\text{-}23)$$

where

$$\left(\frac{\partial\sigma}{\partial\Omega}\right)$$

is the differential scattering cross section for the particular process involved (CARS, LIF, DFWM,etc.) and N_{vJ} is the number of molecules in the initial state involved in the transition.

Finally, we have the fraction of the total number of molecules – N_s – which are in a given vibrational and rotational state as being

$$\frac{N_{vJ}}{N_S} = \frac{g_J(2J+1)}{Z} e^{\frac{-G(v)}{k_B T}} e^{\frac{-F_v(J)}{k_B T}} \qquad (3\text{-}24)$$

with Z (the "zustandssumme" - sum of states, or partition function) being a constant for a given system, and which will always factor out in the calculations we will do here.

We now focus on the term $F_v(J)$ – rotational energy whose constant – v - depends on the vibrational state. This term arises as follows: As the vibrational level v changes, the moment of inertia also changes, so that the rotational energy does not depend only on the rotational state J, but, to a much smaller degree, on the vibrational state. Thus, a given vibrational level will actually have multiple, very slightly different energies which depend on the rotational state.

3.3.1.1 Temperature Measurement by Spontaneous Raman Scattering

Even with laser excitation, spontaneous Raman scattering is a very weak process. Thus, it is only used, in practice, for molecules at high concentration. For combustion in air, whose nitrogen fraction passes through a flame almost untouched, this especially means nitrogen. Fig. 3.8 gives typical Raman spectra for heated air as follows:

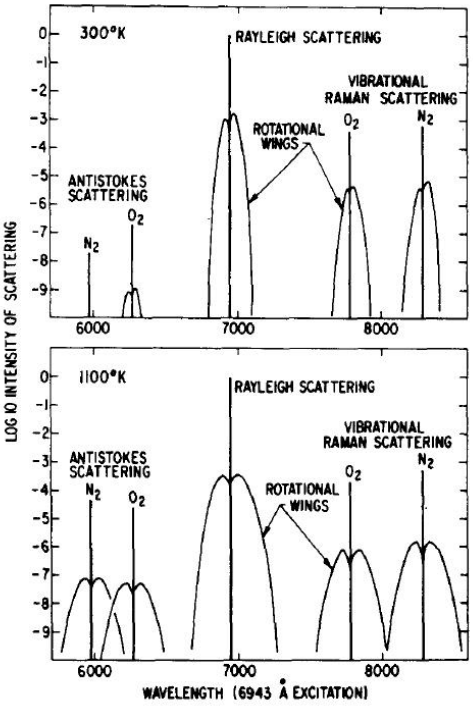

FIG. 3. Raman scattering for air at 300 K and 1100 K.[7]

Fig. 3.8 – Change of Raman Spectra with Temperature (Ref. 34, Fig. 3)
The top graph gives the Raman spectrum at 300K, and the bottom graph gives the spectrum at 1100K. There are two effects of increasing temperature, both resulting from higher temperatures increasing the population of higher-energy states. First of all, the higher energy anti-Stokes vibrational side lobe grows relative to the Stokes side lobe. Secondly, increasingly greater rotational energy within each side lobe causes the vibrational side lobe to broaden.

We see that the Stokes and the anti-Stokes wings remain fixed in location, but change in relative amplitude as the temperature changes, with the anti-Stokes wing growing relative to the Stokes wing as the temperature increases. We know that the two wings are mirror images of each other, with identical oscillator strengths, line positions, and so forth. Therefore, the only way that their relative sizes can change is by changes in the population of the initial states from which they started. The Stokes wing arises from the excitation of a lower energy state, while the anti-Stokes wing arises from the de-excitation of a higher energy state. The Stokes wing has a center frequency ν_S; the anti-Stokes wing has a center frequency ν_{AS}, with each being offset from the centerline by the same amount $\Delta\nu = (\nu_{AS} - \nu_S)/2$. It is separately shown (Ref. 34) that the scattering efficiency is proportional to the fourth power of the frequency. If the area – Φ - beneath each wing is measured, after correcting for whatever differences the optics create for the two wavelengths, then the formula follows:

$$\frac{\Phi_S}{\Phi_{AS}} = \left(\frac{\nu_S}{\nu_{AS}}\right)^4 e^{\frac{-h\Delta\nu}{k_B T}} \qquad (3\text{-}25)$$

which can then be inverted to yield T, since all the other parameters are measured from the spectrum.

The offset of the wings is due to vibrational transitions, which, in the example of a typical case given here, have energies about 0.12 eV, corresponding to about 1300K. Thus, reliance on the Stokes/anti-Stokes ratio becomes impractical below abut 800K because the population of the anti-Stokes wing becomes so small. At this point, it is necessary to consider the rotational spectrum which involves much smaller energy differences. Fig. 3.9 gives a typical rotational spectrum which would reside in the "rotational wings" of the Raman spectrum:

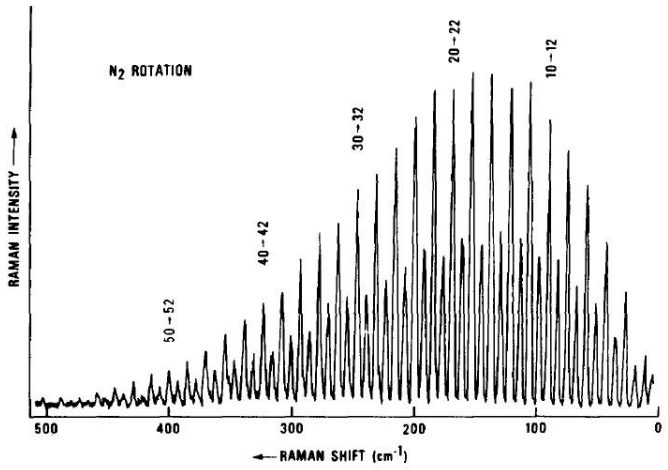

FIG. 4. Stokes N_2 rotational Raman spectrum for an $H_2/O_2/N_2$ flame.[8] The flame temperature is 1988 ± 14 K.

Fig. 3.9 – Nitrogen Rotational Raman Profile (Ref. 34, Fig. 4)
This gives the detailed rotational broadening within a vibrational wing. The lowest energy is at the right, with increasing energy states to the left. The curve exactly follows the Boltzmann distribution, with a peak which is a function primarily of the absolute temperature and the moment of inertia of the molecule.

The numbers above the lines are the rotational quantum numbers – J – whose determination from the spectrum is a well-established part of the spectroscopist's art (Ref. 65). It is possible to infer the temperature either from the peak of the spectral envelope, or from the ratio of line intensities, as follows.

To visualize temperature from the peak of the curve, we begin with an extremely simplified model of the rotational energy as a function of the quantum number, where the rotational energy is given by

$$B \cdot J \cdot (J+1)$$

and B is the product of the greatest moment of inertia and several physical constants. Then the distribution of population among the quantum states – J – will be

$$\frac{N_J}{N_S} = \frac{g_J(2J+1)}{Z} e^{\frac{-BJ(J+1)}{k_B T}} \qquad (3\text{-}26)$$

In the spectrum given, g_J has one single value for even values of J, and another single value for odd values of J. Thus, if we differentiate only on either the odd or the even values of J, the derivative of g_J drops out, and we get that the peak of the J curve, as a function of temperature, will be

$$J = \frac{1}{2} + \sqrt{\frac{k_B T}{2B}} \qquad (3\text{-}27)$$

Thus, the temperature gives the peak of the rotational spectrum and vice versa. In reality, the formula is more complex than this, as it must compensate for varying line strengths, rotational-vibrational coupling, and optical parameters of the measuring system. For a common molecule like nitrogen, line strength and rotational-vibrational coupling are tabulated, while the optical parameters can be calibrated out. Further, at lower temperatures the rotational-vibrational coupling goes away. Another approach to this is to compute theoretical spectra as a function of temperature, and then least-squares fit them to the observed spectrum with temperature as the fitting parameter to get the best estimate of temperature.

If the irradiance of an individual line – $I(N_J)$ can be related to N_J/N_S in the form $Nj(I_J)$, then the ratios of the irradiances of two lines will give - again using the simplified model for rotational kinetic energy:

$$\frac{1}{T} = \frac{k_B/B}{J_1(J_1+1) - J_2(J_2+1)} \ln\left[\frac{N_{J2}(I_{J2}) g_{J1}(2J_1+1)}{N_{J1}(I_{J1}) g_{J2}(2J_2+1)}\right] \qquad (3\text{-}28)$$

In practice, multiple ratios are taken and least-squares fitted with the temperature to the experimental ratios, to get the best guess at temperature.

3.3.1.2 TEMPERATURE MEASUREMENT BY LIF

Laser-induced fluorescence is primarily used to make measurements of species at low concentration, in contrast to Raman scattering which is used for species at high concentration. Raman scattering has a very low sensitivity, but does not require that the exciting laser be tuned to the specific molecule. In contrast, because LIF is a resonant process, the sensitivity is very high, but requires that the laser either be tuned to the specific molecule of interest, or be a powerful broadband laser. In any event, for LIF, the energy levels and spectra of the molecules of interest must be known in advance.

As mentioned before, the basis of temperature measurement is the relative population of different energy states. Laser-induced fluorescence excites molecules out of a state i into a state j, and then observes the intensity of the radiation emitted as the molecule decays from state j to one or more other states k.

For starters, we will represent the equation for the received optical power as:

$$\begin{pmatrix} received \\ power \\ at \\ sensor \end{pmatrix} = \begin{pmatrix} sensor \\ parameters \end{pmatrix} * \begin{pmatrix} molecule's \\ light \\ scattering \\ effectiveness \end{pmatrix} * \begin{pmatrix} incident \\ laser \\ irradiance \end{pmatrix} * \begin{pmatrix} number \\ molecules \\ in \\ initial \\ state \end{pmatrix} \qquad (3\text{-}29)$$

which is a simplification of eqn. 17 of Ref. 34, and will be discussed later. A "molecule" can be monatomic as well as polyatomic. The received power, sensor parameters, and incident laser irradiance can be determined with a high degree of precision, albeit with possible experimental difficulties. If the molecule's light scattering effectiveness can be either determined or factored out, the ratio of molecules in different energy states will give the temperature by Boltzmann's equation.

Just as in Raman scattering, the temperature levels and temperature differences of interest are such that changes between vibrational and rotational states, rather than between electronic states, are what are useful. A typical temperature of 1500K corresponds (from multiplying the Boltzmann constant of 8.61×10^{-5} eV/K by the temperature) to about 0.13 eV, and a change of 10K corresponds to a change of about 0.001 eV – level changes characteristic of the vibrational and rotational modes of molecular motion. While closely-spaced electronic transitions exist in gallium and thallium with these spacings, the literature appears to primarily emphasize vibrational and rotational spectroscopy.

To give a quantitative example of this, at 1500K, for two states which differ by 2 eV - characteristic of electronic transitions - the more energetic state will be populated by a factor of $10^{-6.7}$ of the less energetic state, and a temperature change of 10K will change the population ratio by a fraction of 4×10^{-6}. If the states are separated by 1.2×10^{-2} eV – characteristic of rotational and vibrational modes - the more energetic state will be populated to 91% of the less energetic state. While the fractional change will be the same with a change of temperature, the absolute change and the associated measurability will be greater. If a large number of states are monitored, least-squares fitting will increase the precision of the measurement.

Laser induced fluorescence works by exciting specific level changes in a molecule with laser light in the visible or near-visible range, and then observing the intensity of the emitted light. The spectroscopists have determined – quite exactly - the wavelengths corresponding to changes between specified initial electronic/vibrational/rotational states (svj) and final electronic/vibrational/rotational states (s'v'j'). There are two flavors of laser-induced fluorescence temperature measurement – excitation and fluorescence. One factor to be

remembered is that, while a specific transition is excited, decay and the associated emissions occur over many transitions and wavelengths.

In excitation, a specific ground state is excited to a specific excited state, and the total emission over all wavelengths is monitored as the excited state decays. This total emission will be proportional to the population of the initial state. If the laser frequency is then shifted to a different rotational or vibrational ground state, there will be a different total emission corresponding to the different population of the ground state due to its different energy. A large number of ground states can be so sampled, and the vibrational and rotational intensities least-squares fitted to a theoretical distribution, using the same formulae as were used in Raman scattering.

Fluorescence measurements are performed with a fixed excitation to a fixed upper state - s'v'j' - scanning through the emitted wavelengths as the upper state decays to various lower s''v''j'' states. The intensity at each wavelength will be proportional to the population of the initial excited state. Here, there is the assumption that the upper state and the various lower states will have established a thermal equilibrium. This assumption is not always supportable.

Finally, by using two closely spaced ground states, the "two-line" technique works by illuminating the region of interest with two wavelengths which excite the different ground states to the same final state. The ratio of the total emissions from each again permits calculation of the temperature. Since the measured transitions are the same for both excitations, the uncertainties of quenching and fluorescence efficiency cancel out. The excitations are alternated while emission measurements are made synchronously with the excitations. The excitations have to be separated by a time greater than the greatest quenching time for the emissions, which should not be a significant limitation.

3.3.1.3 Temperature Measurement by CARS

LIF is normally associated with minority species because of the great sensitivity of resonant scattering. Raman spectroscopy – both spontaneous and coherent – uses the major species because the cross-section for Raman scattering - which is non-resonant - is so small. CARS spectra will be qualitatively similar to spontaneous Raman spectra, but differ quantitatively because of the greater nonlinear excitation. Another difference is that, in CARS, only the anti-Stokes spectrum is of use. The reason is that the Stokes spectrum is centered on one of the exciting wavelengths, whose scattering within the apparatus gives a large background noise. Thus, determination of temperature by the ratio of anti-Stokes to Stokes irradiances is not done in CARS. Because the CARS spectrum is so strong, temperature and species are instead determined by the variation of the shape of the spectrum with temperature or species concentration.

Because nitrogen is the major constituent of air, CARS of the nitrogen is the most commonly used application of CARS to temperature measurement. In this case, the relative magnitude of the lower energy and higher energy transitions within the anti-Stokes wing of the spectrum is the measure of temperature.

Temperature measurement using nitrogen begins with theoretically computed spectra, varying with temperature. Fig. 3.10 has typical theoretical nitrogen spectra for a specific experimental setup, for multiple temperatures.

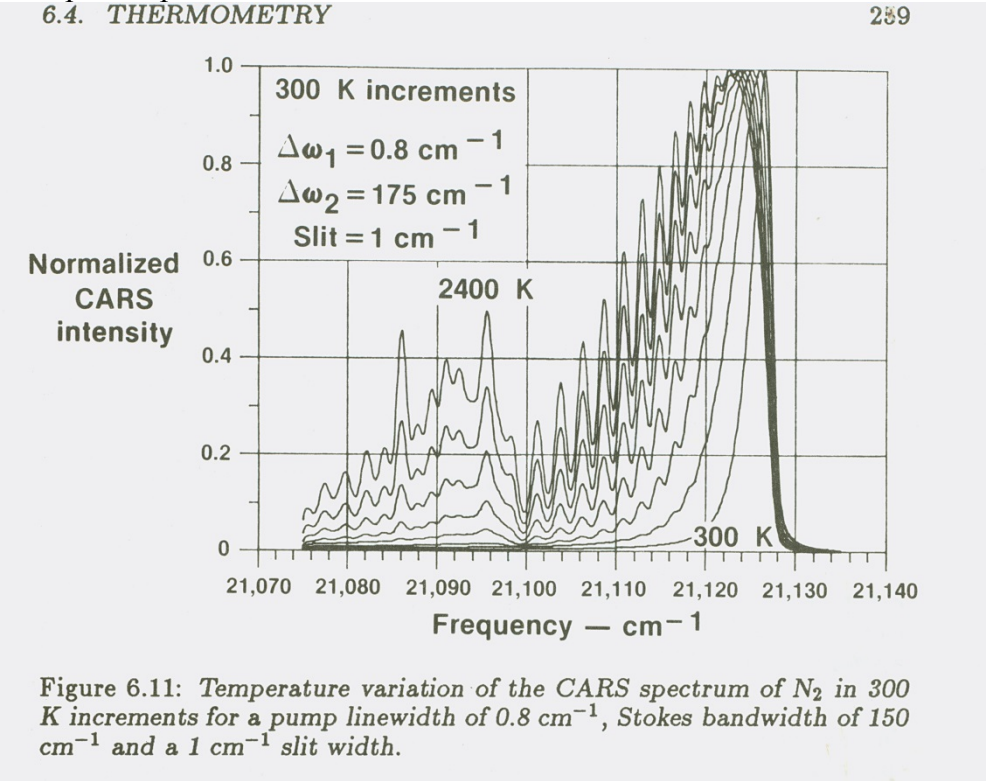

Fig. 3.10 – CARS Spectra Changes with Temperature (Ref. 23, Fig. 6.11)
In this plot, increases of temperature cause the vibrational wing of the spectrum to grow relative to the center, and both the vibrational wing and the center to be broadened by rotation. Such spectra can be computed theoretically, and compared to the observed spectrum to infer the temperature.

In practice, an experimental spectrum will be obtained, and the best least-squares fit to the theoretical spectrum for the same setup is what is used, using temperature as the fitting parameter.

3.3.1.4 Temperature Measurement by DFWM

With DFWM, we are back to resonant excitations, lending themselves to measurements based on minority species. Again, by scanning the wavelength, a spectrum can be obtained which is similar to the LIF spectrum – but not identical - and used in much the same way. Fig. 3.11 compares LIF and DFWM spectra, showing the similarity between the spectra measured by LIF and by DFWM.

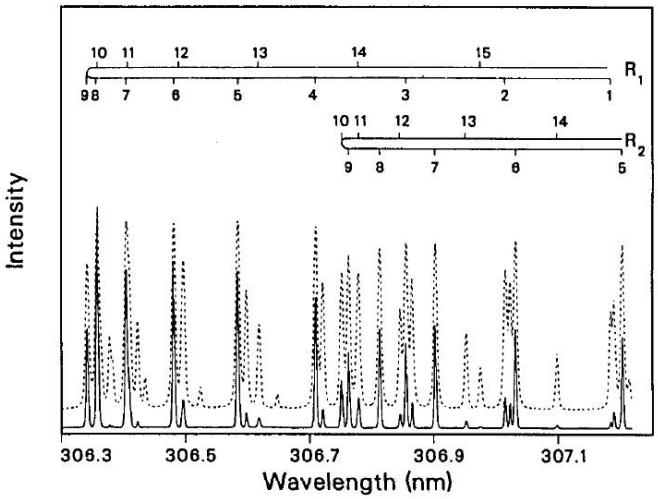

Fig. 2. Simultaneous recording of the DFWM (solid curve) and LIF (dashed curve) signals as a function of doubled dye-laser wavelength. The pump-beam energy is 780 μJ and the probe-beam energy is 74 μJ. For clarity the LIF spectrum is offset with respect to the DFWM spectrum baseline by an arbitrary amount. The vertical scale is in arbitrary intensity units.

Fig.3.11 – Similarity of DFWM and LIF Spectra (Ref. 36, Fig. 2). Because both LIF and DFWM depend on the same molecular absorption phenomena, the spectra will have lines at the same location. This figure slightly offsets the lines for clarity.

As discussed in Ref. 36, the difference between the two types of spectra arises from the fact that line strength with LIF is proportional to the Einstein B_{ij} coefficient for the transition i→j, while the line strength with DFWM is proportional to the square of this same coefficient.

3.3.2 Species Measurement

Generally, there are three types of species measurements for which optical/spectral techniques could be used in a flame:

1) The structure and composition of an unknown material could be determined from its previously unknown spectrum;
2) The presence of a material could be determined by comparing its observed spectrum with a previously determined spectrum;
3) If a material is known to be present, its concentration can be determined by some sort of measurement of the "intensity" of some of the spectral lines.

While (1) – the science of determining molecular structure from spectra (Refs. 37–39, 42) – is a well-established science – it is not part of mainstream combustion research.

Kohse-Höinghaus (abbreviated hereafter as KH) (Ref. 41) begins her discussion of LIF with the statement "A prerequisite for the detection of a radical with LIF is a known absorption and emission spectrum in an accessible wavelength range". A review of the literature shows that this

restriction is not limited to LIF, but applies, across the board, to all the techniques used for species detection in practical combustion measurements.

Thus, identification of species in a flame requires the availability of a library of spectra of the various species of interest. In an earlier time, spectra were catalogued and methodologies for matching observed spectra to catalogued ones were well developed (Ref. 40). More recently, the spectra have been digitized, and are commercially available for semi-automated identification of species (Ref. 42)

Once that the species of interest which are present are determined, only some portions of the spectra are used to determine concentration. These are usually very small portions which, however, are unique to the specific molecules in the system under study. The choice will be made on such criteria as the match of the particular spectral lines to the available lasers, the strength of the transition, etc., and it is at this point that we begin to encounter the differences between the different techniques.

Originally, spectra were observed strictly in emission. While this is still unavoidable in astronomy, excitation by, or absorption of, a strong laser beam allows much better control of the spectral variables.

While Raman scattering has a very low scattering cross-section, it is the one technique which can yield a nearly complete spectrum without knowing, *a priori*, what wavelengths are present. Rothe & Anderson (Ref. 44) give a very succinct explanation of the difference between temperature measurements and concentration measurements by Raman scattering. Temperature measurements are based on the shape of the spectral lines, which are usually rotational lines. , Concentration measurements are based on the intensity of the spectral lines. We end up with the comparison that Raman scattering will give a complete spectrum but with a low cross-section, while LIF and DFWM require knowledge of the lines of interest, but have very large cross-sections. Further, LIF requires, not only that we know spectral lines quite exactly, but that we be able to tune the exciting laser very exactly – to less than a spectral line width – to the exact spectral line we want to excite. In contrast, CARS only requires that we be able to measure a frequency difference precisely– though, admittedly, this usually implies precise control of the "laser" and "Stokes" beams.

3.3.2.1 Species Measurement by LIF

As mentioned earlier, KH (Ref. 41) begins her discussion of LIF with the caveat that *a priori* knowledge of spectral lines is necessary. Additionally, a constant theme throughout her discussion is the importance of quantifying the effects of non-radiative decay from excited states. Given all of these, LIF is used to determine the concentration of species whose presence is known (or presumed) on some other basis.

It was mentioned above that LIF is used to measure species in very low concentration. There are two reasons why a species in low concentration is of interest:

1) Contaminants and pollutants – NO_X, SO_X, CO, etc. – can be significant even when present at very low concentrations;

2) Unstable intermediate species – OH, CH, C_2, CN, etc. – significantly affect the progress of the reaction, even they are present only fleetingly and in low concentrations.

As mentioned earlier, LIF involves excitation of a molecule from a lower electronic/vibrational/rotational state to a higher state, followed by radiative decay to a multitude of lower states, with an associated fluorescence spectrum. If radiative decay, dependent on the Einstein A coefficient, were the only decay mechanism, the intensity of the fluorescence would be directly proportional to the concentration of the species. However, there are a large number of non-radiative decay mechanisms, such that the intensity is reduced in an essentially unpredictable – though measurable - way. Indeed, Aldén (Ref. 43) states that the quenching is typically three orders of magnitude greater than the radiative decay.

The evolution of the LIF technique has led to the use of "saturated" LIF as a way of dealing with these problems (Ref. 41). In saturated LIF, the laser pumping is so great that the excitation to the upper state, and stimulated emission and spontaneous decay from the upper state, are so much greater than the various quenching mechanisms that quenching becomes negligible. Also, since the ratio of the population of the upper and the lower states is forced to a fixed value, the fluorescence intensity becomes independent of the excitation intensity.

The simple concept of pumping from a single lower electronic to a single upper electronic state, and then fluorescing back down to the same single lower electronic state, however, must be modified by the fact that each electronic state contains multiple rotational and vibrational states. In particular, transfer of energy between rotational states is so rapid that the upper state should be considered to become a narrow band of states when excited, radiating back down to a narrow band of states at the lower level. Then designating: the lower and upper lines of the initial excitation as $()_1$ and $()_2$, and the aggregate of the fluorescing upper and lower bands as $()_3$ and $()_4$; assuming the Einstein A coefficients between all the upper and lower bands can be aggregated into a single A_{24}; using the Einstein B coefficients between states 1 & 2; and defining the initial concentration in the ground state as N_0^1 we get (paraphrasing eqn. 7.48 of Ref. 23):

$$\begin{pmatrix}\text{Received}\\ \text{signal}\\ \text{power}\end{pmatrix} = \begin{pmatrix}\text{Optical}\\ \text{System}\\ \text{Constants}\end{pmatrix} * N_0^1 * \frac{B_{12}}{B_{12}+B_{21}} * A_{24} \qquad (3\text{-}30)$$

In this situation, it is apparent that, once the system constants (involving the illuminated volume and the collection efficiency of the measurement system) and the Einstein coefficients are determined (or possibly calibrated out), the received signal power is directly proportional to the species concentration. In order for this to work, too, the spectrometer viewing the emission must be opened wide enough to get the entire band $()_{24}$ – otherwise, the analysis is inapplicable.

As in any technique, saturated LIF has numerous limitations. First of all, the exciting (Gaussian) beam will not be uniform in irradiance, so some of the illuminated volume will not be saturated and will give a signal which is quenching dependent. Skillful optical design has been used to work around this.

Powerful tunable lasers are necessary – Ref. 23 gives spectral irradiances of 10^5 (W/m^2)/nm as being needed. The intense excitation can stimulate spurious reactions which alter the state of the gas under study, thereby undoing laser diagnostics' advantage as being a non-intrusive means of measurement. More interestingly, the powerful illumination can stimulate a Raman signal in the majority nitrogen constituent, which, in some cases, can overlap the fluorescent emission being measured.

3.3.2.2 Species Measurement by Incoherent Raman Scattering

As mentioned earlier, the weak signal generated by incoherent Raman scattering restricts it to measurements of the species which are present at higher concentration, but a laser of any wavelength can be used. Also, a single shot will give a complete set of spectra of all the species present – though only the spectra of the species present in high concentration may be intense enough to be measured. Further, the intensity of the scattered signal is not subject to quenching, as is the case in LIF. Finally, the use of Raman scattering makes the vibrational and rotational spectra – inherently infrared and microwave – accessible to analysis by optical techniques in the visible band.

The temporally and spatially precise measurement of the proportions of the majority species – oxygen, fuel, carbon dioxide, water – is critical to following mixing and the volumetric reaction rate in high-intensity combustors.

The fundamental relationship for density measurement of a specific constituent – *i* - by Raman scattering can be paraphrased from Ref. 23, eqn. 5.24 as:

$$\begin{pmatrix} Scattered \\ Raman \\ Power \\ -P_r \end{pmatrix} = \begin{pmatrix} Incident \\ Beam \\ Power \\ -P_i \end{pmatrix} * \begin{pmatrix} Optical \\ System \\ Design \\ Constants \end{pmatrix} * \begin{pmatrix} Species \\ Concentration \\ -n_i \end{pmatrix} * \begin{pmatrix} Species \\ Scattering \\ Cross-section \\ -\left(\frac{\partial \sigma}{\partial \Omega}\right)_i \end{pmatrix} \qquad (3\text{-}31)$$

The incident and scattered beam powers can be accurately measured, and the optical system design constants can be calibrated out in cold flow, working with nitrogen. The species scattering cross-sections are specific to specific lines of the spectra of specific species, and tabulations exist (examples are table 5.1 of Ref. 23 & table 4, Ref. 44). A problem arises that the weighting of the different lines of a spectrum will change as temperature changes, which is, after all, the basis of temperature measurement by Raman scattering. Fortunately, most practical combustion work is done with air, the majority of which is nitrogen which reacts only minimally, and so maintains a nearly constant level through the flame. This allows the density of the species of interest to be determined by taking the ratio of its vibrational lines to the intensity of nitrogen's vibrational lines. The ratio of vibrational lines is taken, because the weighting of vibrational lines changes much less with temperature than do the weightings of rotational lines.

3.3.2.3 Species Measurement by Coherent Raman Scattering

Coherent Raman scattering is a slightly different thing. We remember that, with coherent Raman scattering, the spectrum is constructed by heterodyning a "Stokes" beam against a "laser" beam,

and observing the difference frequencies at which molecular resonances give a strong, off-axis beam. If the Stokes beam is a broad-band laser, then an entire spectrum can be generated with a single shot. An intermediate procedure is to have multiple Stokes beams of different colors.
Eckbreth (Ref. 23, section 6.5) points out that species concentration with CARS can be measured in two ways: by the integrated intensity of a portion of the spectrum of the species of interest, or by the change of shape of the spectrum as the ratio of resonant signal (at a specific spectral line) to background level (from non-resonant background) as a function of concentration.

The integrated intensity is the easier to understand. The intensity of a scattered wavelength is proportional to the square of the nonlinear component of the resonant susceptibility, which component is, itself, proportional to the gas density. More rigorously, per Ref. 24, p. 84, the resonant susceptibility is proportional to the difference between the population of the upper states and the lower states at the resonant frequency. Then, as the portion of the CARS spectrum of interest is scanned, the intensity of specific lines will be proportional to the gas density. Integration of the spectral band gives a signal proportional to the square of the density.

The above assumes that the resonant spectral lines stand out clearly from the non-resonant background created by other molecules and modes. If not, the spectral line shape will change as the ratio of the resonant CARS signal to the background signal changes. It turns out that this change of line shape, itself, can be used to determine concentration, as shown in the following Fig. 3.12:

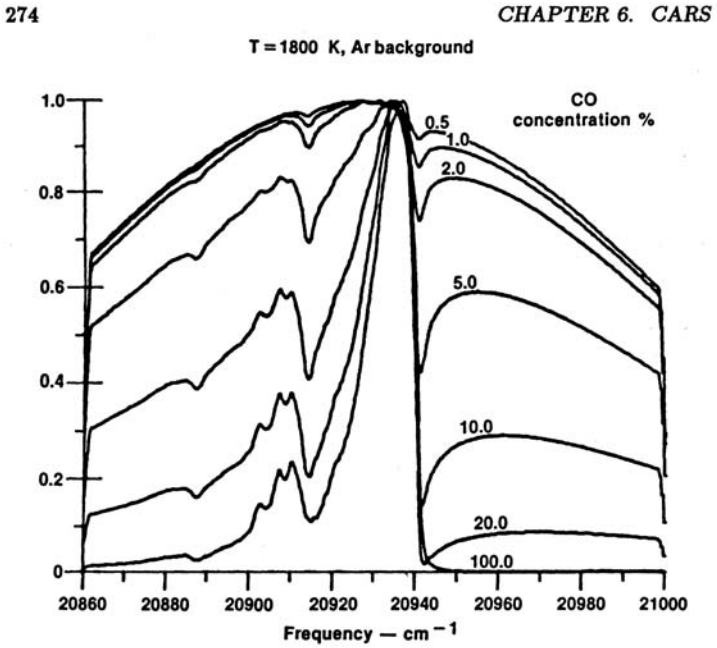

Fig. 3.12 – CARS Spectrum Shape Variation with Temperature (Ref. 23, Fig. 6.22). Each of the computed curves of signal vs. frequency is normalized to the peak value. The ratio of the peak - at about 20930 cm^{-1} - to the magnitude at another chosen frequency is uniquely a function of the concentration.

The figure above, taken from Ref. 23, shows how a CARS spectrum of one species will change shape as concentration changes. A fuller description of the line shape technique is given in Ref. 47.

Reviewing the literature, it appears that the line shape technique has been applied much less than has the line intensity technique. Progress seems to have been concentrated more on finding spectral regions which remain distinct rather than fighting with indistinct lines. Developments in exploiting pure rotational spectra seem to have dominated here (Ref. 45).

3.3.2.4 Species Measurement by DFWM

KH (Ref. 41) states that degenerate four-wave mixing can be considered to be a variant of CARS, in which all of the beams have the same frequency, and resonances are identified by the reflection of the probe beam rather than the emission of the anti-Stokes beam. As such, ". . the main characteristics of DFWM closely resemble those of CARS." Interestingly, even though the basic analysis of DFWM is written in terms of a single wavelength, in actuality it can be used with a broadband laser to obtain a complete spectrum with a single pulse.

Ref. 46 is cited by many publications in the field as one of the definitive studies of the subject of species measurement by DFWM. One of the major conclusions of this study was that saturating DFWM was clearly superior to unsaturated in terms of practically every experimental consideration. It was found to be insensitive to variations in laser irradiance, to variations in absorption, to variations in line width, and to provide superior spatial resolution. About the only problem which seemed to be made worse by the use of saturated DFWM was that of "thermal gratings". A thermal grating is a phenomenon created by the high heat release associated with the same high optical absorption. It turns out that the heat release creates additional refractive index variations which give spurious reflections. Ref. 46 experimented with this, and determined that "cross polarized" configurations, in which a pump and the probe beam were polarized one way, and the other pump beam and the signal beam were polarized perpendicularly, suppressed this effect.

Having said this, these refractive index variations would seem to be co-located with the regions of high absorption, and therefore would change the reflectivity, but not the wavelength, of the Bragg grating. I have extensively reviewed the literature, and have not been able to figure out why this creates an error.

We had, as before, the signal as a function of number density of the species <u>in a specific ground state corresponding to a transition 1→2</u>. This is NOT the total density of that species, but only the density of those in a particular state.

$$I_{signal} \propto \left(\left|\mu_{12}\right|^3 N^2 \left[\frac{T_2}{T_1}\right]^{1/2} I_{pump}^{-1/2} \right) I_{probe} \qquad (3\text{-}32)$$

From knowledge of the temperature, the Boltzmann distribution lets us know the fraction of the total molecules which are in this state, and so we can determine the total number density of the specific molecule.

4. INTERFEROMETRIC MEASUREMENTS

4.1 BACKGROUND

The initial use of interferometry in gas dynamics was to measure gas density in compressible (high Mach number) flows. While the picture was two-dimensional, properly structured test setups yielded significant insights into many flow phenomena. The greater coherence length of laser illumination would certainly have simplified this type of interferometry, but progress has not gone in this direction. As pointed out in the previous chapter, density can now be mapped out in three dimensions by CARS, giving a much superior result.

The chief usage of laser interferometry in flow and combustion has become velocity measurements, under the names of Laser Doppler Velocimetry (LDV) or Laser Doppler Anemometry (LDA). In this note, the abbreviation LDA will be used. The volume probed can be in the range of a few cubic millimeters, the range of velocities is practically unlimited, and the flow is undisturbed by the measurements. Of course, this is countered by the complexity and expense of setting up the measurement apparatus, not even considering the problems caused by things which block or deflect the light beams, imperfections in the optics, and the electronic problems of shot noise with a weak signal.

4.1.1 The Basic Phenomenon

4.1.1.1 Basic Description

The fundamental arrangement for LDA, as most commonly implemented currently, is depicted as follows:

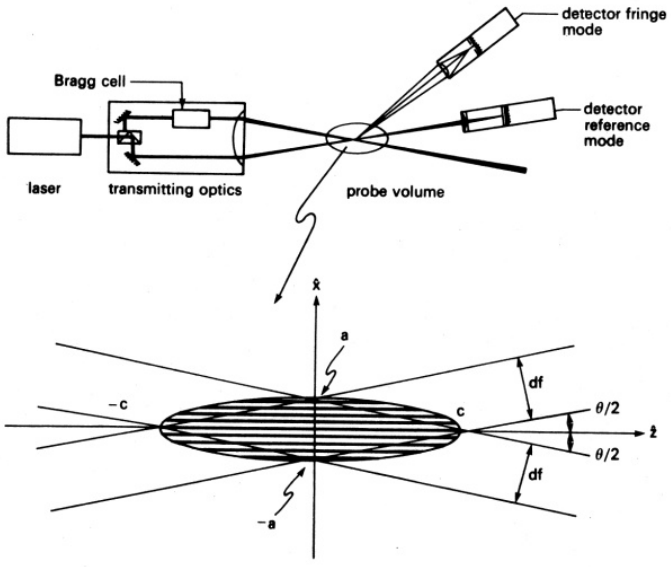

Figure 1-2 Optical configuration of typical LDA.

Fig. 4.1 – Schematic of LDA (Ref. 48, Fig 1.2)

The beam from the laser is split into two beams, one of which is frequency-shifted by a Bragg cell. They are then combined in the probe volume to form interference fringes. Particles passing through the probe volume scatter light at a frequency proportional to their velocity perpendicular to the fringes, which is measured by the "detector – fringe mode".

in which the flow is seeded with particles which scatter the light. The scattered light will be modulated with a frequency – f - proportional to the velocity component normal to the fringes – u – such that

$$f = \frac{2 \cdot u \cdot \sin\left(\frac{\theta}{2}\right)}{\lambda} \qquad (4\text{-}1)$$

where θ is the angle between the direction of the two beams.

Section 2.3.3 described the use of Doppler-shifted Rayleigh scattering in a similar measurement technique, but which did not require seeding. Yet another alternative technique which does not require seeding, but which instead uses the interference of laser-induced fluorescence in a similar geometry, is described in Ref. 50, and will be discussed later.

A consistent theme in the literature is differentiation between "fringe" and "Doppler shift" velocimetry. "Fringe" velocimetry is presented as arising from the seeding particle scattering a burst of light each time it passes through an interference fringe, while "Doppler shift" velocimetry is presented as arising from the heterodyne of the Doppler-shifted scattering of the two beams by the moving particle. When the two paradigms are analyzed, being represented by putatively different physical models, the identical frequency relation results.

4.1.1.2 A Digression to Clarify

The fact that the separately-derived frequency relationships for "fringe" and for "Doppler shift" are the same raises the suspicion that they are really different ways of representing (and implementing) the same phenomenon. To get some insight, consider the situation for which $\theta=\pi$, so that a left-traveling wave and a right-traveling wave form the fringes, and a frequency of $2u/\lambda$ is predicted.

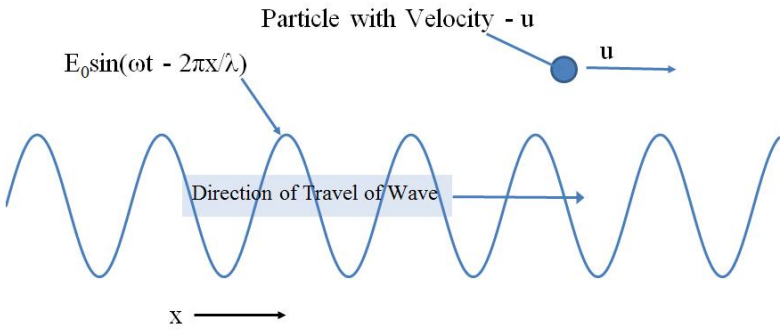

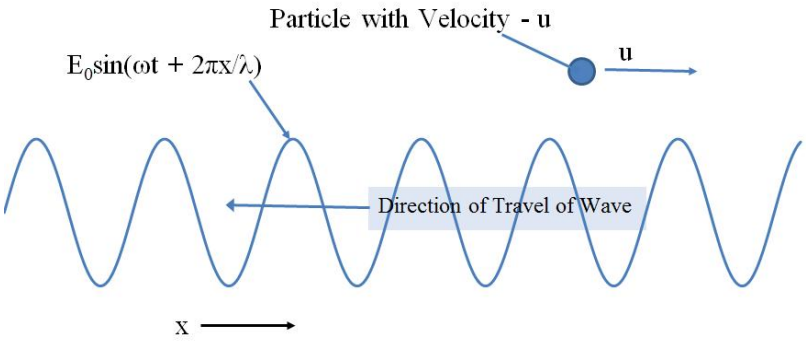

Fig. 4.2 – Generation of Beat Frequency Between Two Scattered Waves

For the right-traveling wave, we have the amplitude of the wave given by

$$E = E_0 \cdot \sin\left(\omega t - 2\pi \frac{x}{\lambda}\right) \qquad (4\text{-}2)$$

and, for the left-traveling wave

$$E = E_0 \cdot \sin\left(\omega t + 2\pi \frac{x}{\lambda}\right) \qquad (4\text{-}3)$$

with the trivial dispersion relationship

$$c = \frac{\omega\lambda}{2\pi} \qquad (4\text{-}4)$$

Adding the two fields gives the unexceptionable result for the total field

$$E = 2E_0 \cdot \sin(\omega t) \cdot \cos\left(2\pi \frac{x}{\lambda}\right) \qquad (4\text{-}5)$$

that is, simply a standing wave – or interference fringes – with a spacing of λ/2.

If a particle with a right-traveling velocity – u – is now placed in this field, it will be subjected to, and scatter, a field of

$$E_0 \cdot \sin\left(\omega t - 2\pi \frac{x+ut}{\lambda}\right) \qquad (4\text{-}6)$$

from the right traveling wave, and a field of

$$E_0 \cdot \sin\left(\omega t + 2\pi \frac{x+ut}{\lambda}\right) \qquad (4\text{-}7)$$

from the left-traveling wave, which add up (after some trigonometric manipulation) to

$$2E_0 \cdot \sin(\varpi t) \cdot \cos\left(2\pi \frac{u}{\lambda} t - 2\pi \frac{x}{\lambda}\right) \quad (4\text{-}8)$$

This is simply a carrier of frequency ω, amplitude modulated by an envelope with an angular frequency of

$$\omega_d = 2\pi u/\lambda \quad (4\text{-}9)$$

which goes peak to peak in a time $(\lambda/2)/u$ or a peak-to-peak frequency of $2u/\lambda$ - as expected from the Doppler shift model. However, there is also a spatial modulation, or fringe spacing (which we had seen before) of λ, which goes through an extreme at each

$$w = \lambda/2 \quad (4\text{-}10)$$

At a time $(\lambda/2)/u$, for the same phase shift, x has changed $(\lambda/2)$ – the fringe spacing, exactly as is assumed in the fringe model. Thus, we see that the two models – Doppler shift vs. fringe – both arise from the change of phase of scattered light as the particle moves. The modulation can also be interpreted as a traveling wave with a velocity equal to u – the particle velocity – which is a way to visualize the reduction of data from the multicolor, multiaxis measurement rigs which will be discussed later.

Perhaps the equivalence is obvious, but the literature never discusses this equivalency. Even though the two interpretations come from the same mathematics, implementation per the two paradigms can have quite different practical effects, as will be shown later.

4.1.1.3 Ambiguity

A glance at the formulae derived above shows that they cannot distinguish between positive u and negative u. If one of the beams is frequency shifted by an amount $\delta\omega$, by a Bragg cell or a moving grating, the frequency-velocity relationship becomes

$$\omega_s = \delta\varpi + 2\pi \frac{u}{\lambda} \quad (4\text{-}11)$$

so that a zero velocity has a nonzero signal frequency, with negative velocities decreasing the signal frequency, and positive ones increasing it. While some care must be used in matching the laser beam of a multi-color laser to the Bragg cell wavelength to avoid false frequency shifts, these problems have not proven to be overwhelming. (Ref. 56)

4.1.1.4 Three-Dimensionality

Because flows of practical interest have three components of velocity, three-dimensional measurements are needed. With steady flows, this was originally achieved by mounting the optical system on a rotatable carriage (with, of course, a considerable bit of good mechanical design necessary to assure that all of the critical alignments were maintained). This was quickly abandoned, with lasers of different wavelengths instead being used for each axis. A typical arrangement (Ref. 52) is as follows:

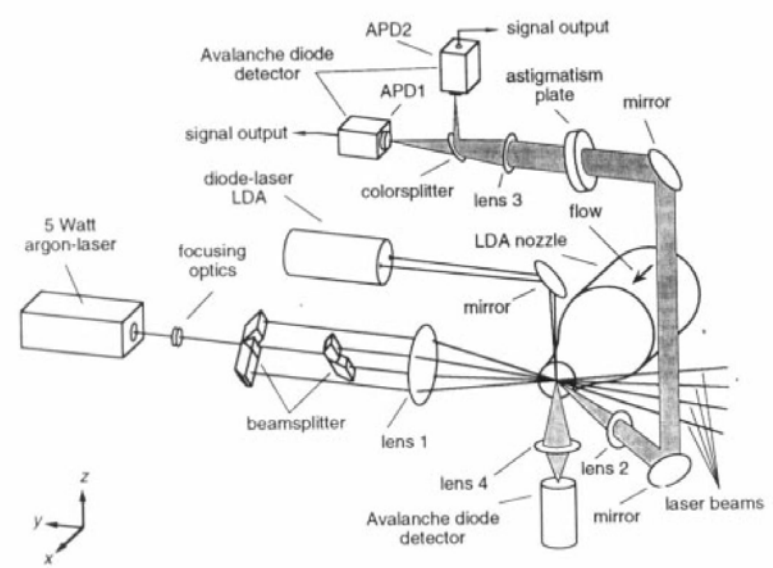

Fig. 4.3 – Multi-Wavelength 3-D LDA Setup (Ref. 52, Fig. 3)
In this case, the three components are measured by three colors – two from an argon laser, and one from a shorter-wavelength diode laser. The argon laser beam is split into two perpendicular interference patterns of different wavelengths by dichoric beamsplitters, which are then distinguished by their wavelengths to give two components of velocity. The third component of velocity is directly measured by its own set of interference fringes.

In this particular case, the diode laser was a specially developed one whose shorter wavelength and small size were optimized to make measurements in the boundary layer. More commonly, three wavelengths, such as 514.5, 488.0, and 476.5nm. - as could be taken from a single argon-ion laser - can be used. Additionally, mirrors seem to be rapidly giving way to fiber optic arrangements, which keep their alignments much better.

It is also possible, by a good understanding of optics, to get a 3-dimensional velocity measurement with a single-wavelength laser. Fig. 4.4 depicts one such arrangement.

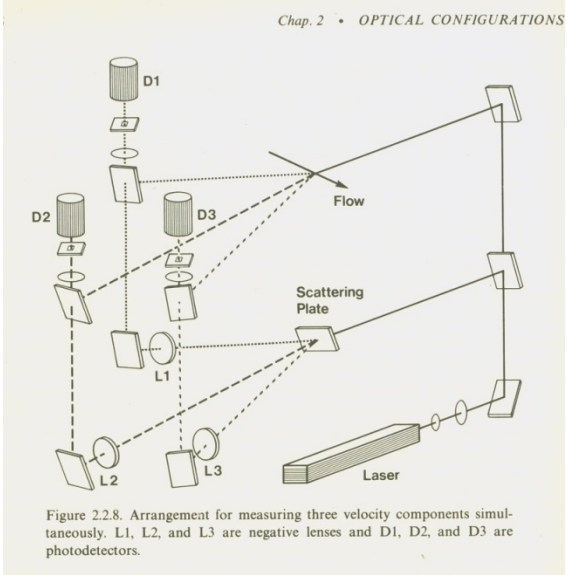

Figure 2.2.8. Arrangement for measuring three velocity components simultaneously. L1, L2, and L3 are negative lenses and D1, D2, and D3 are photodetectors.

Fig. 4.4 – Single-Wavelength 3-d LDA Apparatus (Ref. 51, Fig. 2.2.8)

This figure depicts another approach to 3-d velocity measurement which was used for a short period of time, and deserves some discussion because it uses the basic concepts developed in section 4.1.1.2 in a slightly different way. By dint of a sophisticated understanding of optics, it manages to measure three components of velocity using a single wavelength, as follows:

If we return to the basic concept, we can view the underlying mechanism of LDA as being the mixing of two Doppler-shifted beams, which – in the example developed in 4.1.1.2 – are Doppler-shifted in opposite directions. The mixing gives the beat frequency proportional to the velocity, as given in equation 4-8, of

$$2\pi u/\lambda$$

If, instead, there were only one Doppler shifted beam, which was heterodyned with an undisturbed beam, we would still get a beat frequency, albeit only of half this value. This beat frequency would be gotten by mixing the two beams on the viewing port of a detector, instead of in the flow volume at the point of measurement. There is a trade-off here: When the two beams intersect and create fringes, the component of flow being measured is quite well-defined – perpendicular to the fringes – and the location of the measurement is well-defined – the tiny volume where the fringes are created.

By <u>not</u> intersecting the beams in the flow volume, we remove the specificity of position and of direction, and make 3-dimensional measurement possible. First of all, Doppler shifted scattering arises along the full length of the laser beam's trajectory through the moving fluid. Each scattering particle serves as a point source of the illumination it is exposed to, radiating Doppler-shifted light in all directions. In order to choose a specific <u>location</u>, the detector's viewing is focused at the particular point on the beam of interest, re-introducing a measurement at a specific location. However, the viewing is at an unknown angle to the unknown direction of the flow, but at a known angle to the direction of the laser beam. Gupta & Lilly (ref. 49, p. 204) show that the <u>measured</u> Doppler shift of the scattered beam depends only on the projection of the vector

difference of the incident and scattered beams on the flow velocity vector, and this vector difference is known. A three-dimensional velocity measurement is then made by viewing the same point at multiple viewing angles and so with multiple vector differences, which vector differences must not be coplanar. The different projections on to the velocity vector can then be measured, and then resolved into the three perpendicular components of velocity.

This is exactly what is done in the 3-D apparatus shown in Fig. 4.4. The scattering from the incident laser beam is viewed at three different angles (top part of the figure), and the detected beam is mixed with the three unshifted light beams scattered by the scattering plate (bottom part of the figure) on the three detectors, each of these giving a component of the velocity. These three components can then be resolved into the three perpendicular components of velocity.

4.1.1.5 Laser Induced Fluorescence – Not Quite Interferometry

The techniques described up to now all depend on small particles in the flow to scatter the light. If we think back to the discussion of laser induced fluorescence as a form of scattering, it would seem that the extremely narrow bandwidth involved might be put to use.
Hansen (ref. 50) depicts such an arrangement, as follows:

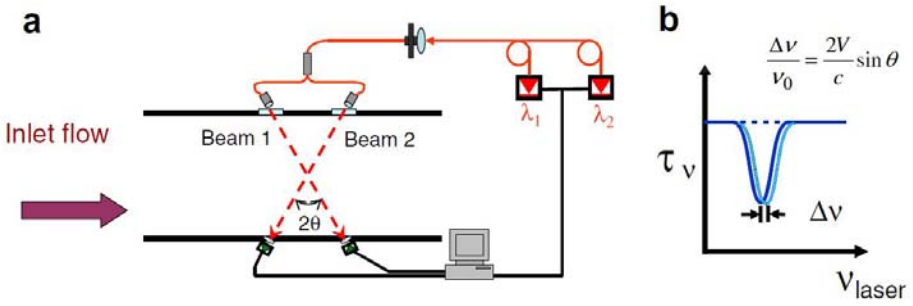

Fig. 35. (a) Schematic of a laser-absorption sensor to determine velocity via the Doppler shift of the two absorption lineshapes; (b) illustration of shifted lineshapes.

Fig. 4.5 – Molecular Scattering LDA (Ref. 50, Fig. 35). The left panel shows that beams 1 and 2 are separately adjusted in wavelength to each give the peak absorption. As shown in the right panel, because of the Doppler shift between the two beams, the absorption peak of the two beams will differ by an amount proportional to their velocity.

As shown, the Doppler shift between the upstream and the downstream running beams is a measure of the velocity. Ref. 50 does not state how the difference is measured, but measuring the heterodyne between the two beams when they are mixed on the face of a detector would seem to be a very sensitive and precise way of making the measurement. Alternatively, the shift between the peaks if both beams are fed into a Fabry-Perot etalon could also be used. As depicted, the system cannot distinguish between positive and negative velocities. In the hypersonic flow application described in Ref. 50 flow reversal is not a consideration. It is not obvious whether Bragg shifting one or both beams would be workable – it is possible that the beam would be detuned from the fluorescing wavelength.

4.2 APPLICATION AND PROBLEMS

4.2.1 Turbulence and Optical Processing

LDA has unique capabilities vis-à-vis turbulence, albeit with more complexity than seems obvious at the start. Turbulence is characterized as velocity fluctuations around a mean velocity, so it would be reasonable to expect that, when measured by LDA, turbulence could be measured by the broadening of the Doppler scattered signal, and this is, indeed, the case. Turbulence theory, however, demands more extensive statistics than this. While the spectrum of the fluctuations at one point (by the Wiener-Khinchin theorem) is the Fourier transform of the autocorrelation of the velocity fluctuations, turbulence theory also uses the cross-correlation of velocities at separated points, as a function of separation. Both optical and electronic techniques have been used to measure these.

One of the first optical methods of measuring the spectrum of the scattered Doppler signal used a Fabry-Perot interferometer , as shown in Fig. 4.6.

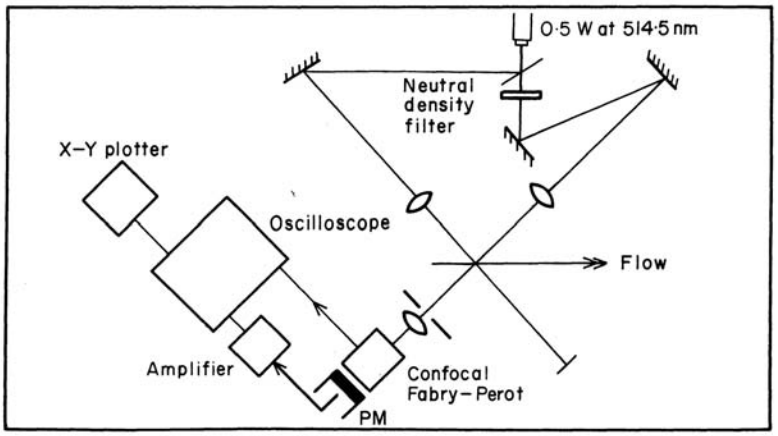

Fig. 4.6 – Fabry-Perot Bandwidth Measurement (Ref. 53, Fig. 6.23).
The device marked "PM" is the photomultiplier that measures the output of the Fabry-Perot etalon. The other (unmarked) line leading to the oscilloscope is a readout of the driver of a piezoelectric actuator which moves one of the mirrors of the etalon. In this way, the etalon is scanned across the spectrum of scattered light. By plotting the displacement of the moving mirror (which is equivalent to measuring the position of the resonance on the Doppler spectrum) vs. the magnitude of the photomultiplier signal, the shape of the Doppler spectrum can be determined.

From the optical viewpoint, the strength of the Fabry – Perot interferometer – its great sensitivity – is also a weakness. The weakness is that the system is extremely sensitive to vibrations, misalignments, and instability of the laser frequency. Ref. 53 makes the point that this arrangement is applicable to high velocities, with essentially no upper bound on velocity, but with stability problems at lower velocities. However, at lower velocities electronic means of frequency measurement are workable up well into the range of Doppler shifts where Fabry-Perot becomes usable.

In order to understand this apparatus, we must turn our thinking around from the development given earlier in this chapter, which was focused on analyzing the envelope of the signal resulting from the heterodyne of two optical waves – an "amplitude modulated" approach. Instead, thinking in frequency space, the presence of a heterodyne appears as a side lobe or as a broadened spectrum – additional waves with frequencies offset from the main frequency – or a "frequency modulated" approach.

If the combined waves are fed into a Fabry-Perot interferometer which has an adjustable length, a peak signal will be observed whenever the length is resonant with a peak of the Doppler frequency spectrum. If the peak is broadened by random fluctuations of velocity, the variation of the output will be related to the amplitude of that part of the peak. In the case of the apparatus depicted in Fig. 4.6, this was done by moving the mirror with a piezoelectric actuator which was driven by a sawtooth voltage. An x-y presentation on an oscilloscope was used to view the spectrum, but nowadays we would expect electronic recording and signal processing. Normally, the turbulent velocity fluctuations are much less than is the mean flow velocity, so that flow reversals are not a concern. (The few cases which are such as to be too slow to be measurable by Fabry-Perot, as will be discussed shortly.)

We need to see what are the demands on such an optical system. The literature makes oblique references to the idea that such measurements are demanding optically, but I have not found any specifics reported. If we consider fluid dynamic measurements of a 27 m/sec flow (60 mph) being made with a 514 nm laser, the Doppler shift will be 5.45×10^{7} cps, while the frequency of the carrier is 5.84×10^{14} cps. (CPS is used rather than Hz to avoid the ambiguity of cyclic vs angular frequency). If the turbulence is 0.1 of the mean flow, the additional Doppler shift due to turbulence will be 5.45×10^{6} cps, and the maximum frequency shift will be about 6×10^{7} cps. Allowing for an available measurement range of some small multiple of this – 2 will be assumed here – requires a free spectral range of 12×10^{7} cps. If we wish to measure the turbulence to within 0.1 of its own level, the FWHM of the cavity will need to be no more than 5.45×10^{5} cps. Putting all these together (ref. 54, p. 109) means that the cavity length must be at least 1.25 meters, with a finesse of 220, or a Q of 1.1×10^{9}. This, for instance, would be met with a reflectivity of 99% at one end, and a reflectivity of 90% at the other end – well within the capability of optical technology.

Measurement of a velocity fluctuation of 0.27 m/sec (the precision which 0.1x0.1x27 m/sec involves) involves varying the length of the interferometer and observing the change of transmitted irradiance, which will correspond to the fraction of time that fluid particles are at the corresponding velocity. Notice that peak tracking is not involved – only knowing the change of the peak transmission resulting from a known change of length, which known change of length corresponds to a known change of flow velocity. In the present example, the length change of a 1.25 meter Fabry-Perot interferometer, to change the resonance by 0.545×10^{6} cps when it initially had a resonance of 5.14×10^{14}, comes out to length change 1.33×10^{-9} meters which must be measured. Compared to the 514×10^{-9} m. wavelength of the light, it becomes plain that a fairly demanding measurement is involved here. Indeed, Duranni (Ref. 51, p. 105) states that a resolution of 10^{6} cps is about the best resolution that can be obtained from a confocal Fabry-Perot etalon.

Thus, we can see why Hansen (Ref. 50) states that the technique is applicable only to higher velocity flows, within which both the mean velocity and the turbulent fluctuations are greater.

4.2.2 Self Mixing

There is an alternative optical means of demodulation which will work with very low velocity measurements. If the Doppler shift is so small that it lies within the linewidth of the original laser beam, the shifted beam can be fed back into the laser cavity and will mix with the laser beam in the cavity, giving a Doppler modulation that can be measured with a photodiode or in the driving current of a semiconductor laser. Ref. 55 describes such a technique, which is sufficiently sensitive that it has been used to measure blood flow.

4.2.3 Turbulence and Electronic Processing

Up till now, this discussion has treated the measurement problem as being one of measuring a long, continuous plane wave. In reality, the scattered wave is far from this, which restricts the utility of the LDA/LDV even further, whether the measurement of the Doppler shift be done by optical or by electronic means. The chief problem is the intermittency of the scattered signal due to the fact that the passage of individual particles through the crossed beams gives an intermittent output, when particle loading is low. (With a high particle loading, such that there are always multiple particles in the field of view which are incoherently scattering to the detector, a "pedestal" of steady illumination lies underneath the Doppler scattered signal.)

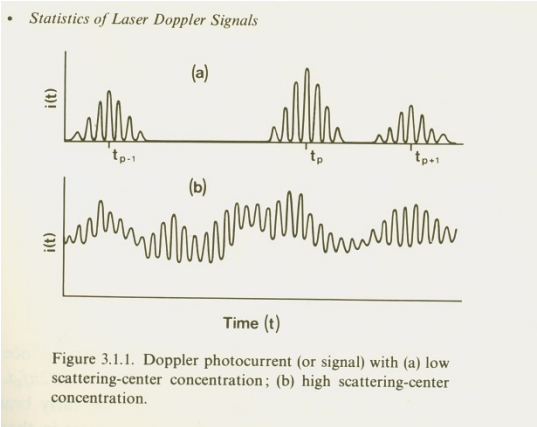

Fig. 4.7 – Intermittency of Turbulence Measurements (Ref. 51, Fig. 3.1.1). The top panel shows the signal expected when only one particle is in the measuring volume at a time – the signal intensity will consist of short bursts of pure signal. The bottom panel shows that, when many particles are in the measuring volume at the same time, the incoherent addition of the multiple sinusoidal scattered signals will give a "pedestal" with a varying, but continuous, sinusoid superposed.

Also, the interference pattern is not one of two infinite plane waves, but the interference at the waist of two Gaussian beams.

Low particle loadings are more characteristic of the situation in combustion and gas dynamic studies, so the problems associated with these will be further discussed. One of the prices paid for the precise location and small measurement volume of LDA is that a particle will only intercept a small number of interference fringes, and so only give a short burst of signal. The practical effect of this is to broaden the Doppler spectrum, whether the flow is laminar or turbulent. The necessary signal processing is referred to as "burst signal processing" (Ref. 58, pp. 467-490).

If the sensing volume of the LDA has N_σ fringes, then Ref. 53 (after much labor) concludes that the ratio of the transit time induced broadening of the frequency – σ_F - to the mean Doppler frequency – ω_D – is given by

$$\frac{\sigma_F}{\omega_D} = \frac{1}{2\sqrt{2\pi}\ N_\sigma} \qquad (4\text{-}12)$$

(Ref. 53, p. 207). Refs. 48 and 56 indicate that this is the most significant source of spurious broadening.

Actual measurement of the frequency of such short bursts is different from normal signal processing. For instance, the Fabry-Perot technique discussed earlier tacitly assumes a signal of consistent amplitude at each frequency, so that a change of amplitude of the transmitted signal comes only from detuning of the cavity from the peak of the velocity distribution. Differing amplitude signals from different sized particles will make the Fabry-Perot technique even less effective.

The electronic devices used to measure the velocity in this case are called "burst processors". Typically, these have an amplitude-gated input, such that an input below a certain level, such as from shot noise, will be ignored. The input is high-pass filtered to give it an average near zero, and then the zero crossings of each burst are measured. The duration of the signal is also measured, so that the frequency, and so the velocity, can be derived. The time of successive bursts from some starting time can also be recorded, for an autocorrelation technique which will be discussed later. Ref. 51, sec. 6.3 gives the details of how such a circuit can be implemented.

Such an intermittent sinusoid, as shown in the figure on the previous page, introduces additional sources of error. One of the more subtle ones is "velocity bias" (Ref. 56). Velocity bias is an error which arises from the fact that, in a given length of time, a higher velocity flow will transport more particles through the measuring volume than will a low velocity flow. Thus, when statistics are accumulated, they will be biased toward the higher velocity. The standard technique to compute the velocity correctly (Refs. 48, 51, and 56) accumulates i measurements of velocity – u_i - each measurement having an associated number of zero crossings – q_i - and measurement duration - δt_i. Then the properly weighted average for the velocity is

$$U = \frac{\sum_i u_i \delta t_i}{\sum_i \delta t_i} \qquad (4\text{-}13)$$

which is cited in Refs. 48, 51, and 56. However, if we note that the *i*-th velocity was originally computed from the *i*-th burst parameters as

$$u_i = w \cdot \omega_{d,i}/\pi \quad (4\text{-}14)$$

and that the scattered light Doppler frequency in each of the *i* measurements is computed by

$$\omega_{d,i} = \pi \cdot q_i / \delta t_i \quad (4\text{-}15)$$

then a bit of manipulation shows that the weighted average for the velocity from a series of velocity measurements is simply

$$U = w \cdot \frac{\sum_i q_i}{\sum_i \delta t_i} \qquad (4\text{-}16)$$

that is, the concept from statistics that the average taken from a large sample is better than the average taken from a small sample.

The individual measurements are still necessary, because it is still necessary to characterize the turbulence by the moments of the velocity distribution. Normally only the first moment is of interest, with more extensive statistical analyses using spatial and temporal autocorrelations, which correlations will be discussed in the next section. Again, the properly time-weighted first moment of the velocity (called the turbulent intensity) is (Ref. 58, p. 473)

$$\overline{u'^2} = \frac{\sum_i \left[u_i - U\right]^2 \cdot \delta t_i}{\sum_i \delta t_i} \qquad (4\text{-}17)$$

These analyses are based on treating each component of velocity separately. Ref. 68 extends them by accounting for all three components of velocity, but the final results obtained are almost identical.

4.2.4 Correlations

Turbulence studies make extensive use of temporal and spatial correlations of the velocity fluctuations around the mean. There is a certain amount of arbitrariness on the definition of "turbulence", because, whether a flow is "turbulent" or "unsteady laminar" is chosen based on the time and distance scale we wish to consider – a situation similar to that in kinetic theory when we are deciding whether matter is to be considered as continuous or atomistic. In this discussion, we will evade this question and simply say that turbulence is what we choose to characterize statistically.

Given this, correlations are used to characterize the fluctuations of velocity – $u_i' = [u_i - U]$ – as given above. If two measurements are taken at times t_1 and t_2, we define an autocorrelation time $\tau = t_1 - t_2$ – and then a temporal autocorrelation $R(\tau)$ becomes

$$R(\tau) = u'(t_1) \cdot u'(t_2) \quad (4\text{-}18)$$

Since the velocity fluctuations are actually continuous variables, we end up with the definition

$$R(\tau) = \int u'(t) \cdot u'(t-\tau) \cdot dt \qquad (4\text{-}19)$$

Autocorrelation and the power spectrum are interconvertable by the Wiener-Khinchin theorem, but in turbulence studies – even back when hot-wire anemometers, having a continuous output, were the primary instrument – autocorrelations have been found to be the more amenable to computation from data.[5] The intermittency of the signal from the LDA makes this even more significant.

A sizable amount of effort has gone into determination of how to use a burst processor output to determine temporal autocorrelations. First of all, the record to be processed must include, not only the duration of a burst - δt – but also its time of arrival – t – with respect to some starting time.

What seems to have become the standard takes two measurements of velocity fluctuation – u'_i and u'_j - taken at times t_i and t_j with burst durations δt_i and δt_j, and computes the autocorrelation as (Ref. 48, p. 490)

$$R(\tau) = \frac{\sum_{i,j} u'_i u'_j \delta t_i \delta t_j}{\sum_{i,j} \delta t_i \delta t_j}; \tau = \left| t_i - t_j \right| > \delta t_i, \delta t_j \qquad (4\text{-}20)$$

The case for $\tau < \delta t_i, \delta t_j$ – that is, the correlation time being less than the larger of the durations – is considered to be $\tau = 0$, and is separately calculated using the formula for the turbulent intensity.

Spatial correlations are also significant in turbulence theory, and have routinely been measured with hot-wire anemometers. This can be defined as

$$R(\tau, \vec{x}, \vec{r}) = \int u(t-\tau, \vec{x}_1) \cdot u(t, \vec{x}_2) \cdot dt; \vec{r} = \vec{x}_1 - \vec{x}_2; \vec{x} = \vec{x}_1 \quad or \quad \vec{x}_2 \qquad (4\text{-}21)$$

There is some vagueness in the terminology here – a correlation with τ=0 would be called a spatial autocorrelation, while with $\tau \neq 0$ would be called a spatial cross-correlation, but these usages are not consistently seen. Ref. 53, p. 355 gives an LDA setup for such measurements – essentially, two replicated measurement volumes separated by the desired distance. Ref. 53 proposes distinguishing the two signals by having them differently polarized; it would seem better to use two different colors, but the matter of spatial correlations is discussed but little in the literature. I was able to find no discussion of correcting for the velocity bias in spatial correlations, but it would seem to use formulae similar to those used in temporal correlations. What would seem to be a much more significant error in combustion applications would be the effect of beam bending by refractive index gradients causing the two measurement volumes to be

[5] In pre-computer, pre-digital circuit days, some very clever tube-type analog circuits were designed to electronically perform the correlations from hot-wire anemometer data.

displaced from their nominal positions, and by different amounts. Again, while spatial correlations have always loomed large in turbulence theory, the LDA literature gives scant attention to the measurement of such correlations.

4.2.5 Other Errors

The most significant other error mentioned in the literature is velocity gradient broadening. This is fairly straightforward – if there is a significant difference in mean velocities across the measuring volume, particles traversing different parts of the measuring volume will give a signal characteristic of their velocity, which would be interpreted as a turbulence signal. This is primarily a consideration when making measurements in a boundary layer.

Fringe curvature at the intersection of the two Gaussian beams would appear to give problems similar to those of velocity gradient broadening, but while I found analyses of these vis-à-vis particle sizing, I found no references relating fringe curvature to velocity measurement.

5. SUMMARY

This survey has discussed applications of laser diagnostics to combustion measurements, with the intent of elucidating the mechanisms of operation and the applications to practice. The explanations were classed by the optical phenomena used to make the measurement. The student of combustion, however, is interested in what he will measure, with how it is measured being only a means to an end. With this in mind, a summary of the measured parameters and the laser-based means of measurement follows, concluding with a précis of some significant optical design problems which were not discussed.

The combustion parameters which are discussed are the following: 1) Temperature; 2) Species identification and concentration; 3) Velocity and turbulence; 4) Particle and droplet size. They are discussed from the point of view of which techniques have become accepted in the mainstream combustion community. Papers presented at the 30th (2005) through the 34th (2013) International Symposia on Combustion were taken as snapshots in time of the best current practice. In particular, the 34th Symposium had a series of "Diagnostics" sessions which gave details on thermometry, species detection, and soot measurements. Several of these papers also included aspects of velocity measurement.

5.1 TEMPERATURE

The 34th Symposium "Diagnostics - Thermometry" session (pp. 3603-3660) had seven presentations. Rotational CARS and two-line LIF were the dominant techniques presented here. There seemed to be no usage of vibrational CARS in these papers, nor of Rayleigh scattering. LIF has become so highly developed that it can be used to follow the temperature history of the charge in a piston engine running at 1000 rpm (Ref. 67). Because the papers were primarily done with combustion in air, all of the rotational CARS analyses exploited the well-known properties of the nitrogen diatomic molecule (N_2) to follow temperature.

5.2 SPECIES IDENTIFICATION & CONCENTRATION

The 34th Symposium "Diagnostics – Species Detection" session (pp. 3531-3602) comprised eight papers. The greatest emphasis seemed to be on high speed measurements in internal combustion engines and in turbulence. Again, LIF measurements seemed to predominate, but cavity ringdown spectrometry was used in the benign environment of low pressure laminar combustion (Ref. 68) to measure species concentration. Cavity ringdown spectrometry, like LIF, requires knowledge of, and precise tuning of the laser to, known spectral lines of the molecule under study.

5.3 VELOCITY AND TURBULENCE

Ref. 67 discussed a technique referred to as cinema particle imagine velocimetry (PIV) which, by the conceptually simple use of both high-speed laser illumination and high-speed image recording, was able to follow the flow processes in internal combustion engines and in individual turbulent eddies. The technique is a refinement of the particle track technique of the past, but with multiple images of a single particle on a film image being replaced with single images of a

particle on successive frames of a high-speed imaging system. The technique was made three-dimensional by use of stereoscopic imagery. A further search through the 30th to the 34th Symposia showed that PIV was being applied to steady state situations where I might have expected LDA to be used, with Ref. 69 being a typical example. However, LDA does still continue to be used to study laboratory-scale steady-state situations (Ref. 70). There seems to have been no use of Doppler-shifted Rayleigh scattering in combustion studies reported in this collection of 34th Symposium papers.

5.4 PARTICLE AND DROPLET SIZE

A survey paper presented at the 34th Symposium (Ref. 71) considers a large number of techniques for measuring the growth of soot from high molecular weight, polycyclic aromatic hydrocarbons, to massive soot. One interesting point is that the simple scattering models break down with the fractal structure of soot in the intermediate stages of growth. For the very smallest size aggregates, an electrostatic sizing technique replaced optical techniques. Because the present note emphasizes optical techniques, these electrostatic techniques will not be discussed.

The measurement of the size of evaporating droplets required a modification of Mie scattering, as reported in Ref. 72. The modification was necessary to eliminate the effects of fluorescence from the evaporated phase, and was found to effectively allow the measurement of evaporating droplets in a fuel spray.

5.5 OPTICAL DESIGN PROBLEMS

There are additional optical aspects of such instrumentation which were not discussed, because they are not unique to this field of application, but are encountered whenever optical devices are used for instrumentation. Admittedly, this distinction is a bit vague – for instance, beam deflection by temperature gradients is not unique to combustion, but is much greater in combustion measurements than it is with non-combustion gas dynamics.

Eckbreth (Ref. 23) has two chapters (3 and 4) entirely devoted to these problems as they apply to temperature and species measurements, and part of a third (Ch. 8) to how they affect measurements of an entire flow field instead of those at a single point. Such matters as separation of the desired signal from spuriously scattered or background light, the effect of shot noise in photomultipliers on the very weak signals often involved, fluorescence in the windows and optics, the need to match etendue through the components of a spectrum measuring system, and 2-d imaging with sheets of laser light instead of focused points, even leading to tomographic 3-d imaging. Similarly, Whitelaw (Ref. 53), for each system that he discusses, gives a detailed discussion of the optical problems – effects of depth of field, optical design to provide optimum light intensity, etc. He extensively evaluates different factors bearing on signal/noise ratio: the effect of photomultiplier noise, the difference between observing a forward and a back-scattered signal, the effects of particle size and density, and numerous other optically-related aspects.

Additionally, other practical considerations can arise. For instance, while the seeding particles in LDA are normally only discussed in terms of how well they might track the flow, Eggins (Ref.

57) points out that in large, closed-circuit wind-tunnel type applications, the seeding particles could wreak havoc on the compressors. This is a non-combustion fluid dynamics situation, where Doppler-shifted Rayleigh scattering might have an application.

A reasonable follow-up would be to explore the detailed optical engineering to make each of the techniques studied work.

REFERENCES

The Proceedings of the International Symposia on Combustion are referred to as "XX Symposium, YYYY", where XX is the number of the Symposium, and YYYY is the year.

1) Turns, S.R.; An Introduction to Combustion: Concepts and Applications, 2d ed.; McGraw Hill, 2000
2) Oran, Elaine S.; "Astrophysical Combustion"; 30th Symposium, (2005) pp. 1823-1840
3) Fristrom, R. & Westenberg, A.; Flame Structure; McGraw-Hill, 1965
4) Gaydon, A.; The Spectroscopy of Flames, 2d ed.; Chapman and Hall, 1974
5) Weinberg, F.; Optics of Flames; Butterworths, 1963
6) Chigier, N.; Energy, Combustion, & Environment; McGraw Hill, 1981
7) Stratton, J.A.; Electromagnetic Theory; McGraw Hill, 1941
8) van de Hulst, H.; Light Scattering by Small Particles; Dover Publications, 1981
9) Bockhorne, H. et. al; "Measurement of the Soot Concentration and Soot Particle Sizes in Propane-Oxygen Flames";, 18th Symposium (1981), pp. 1137-1147
10) Chigier, N. ed.; Combustion Measurements; Hemisphere, 1991
11) Born, M. and Wolf, E; Principles of Optics, 7th ed.; Cambridge University Press, 2001
12) Vaglecio et al; "In Situ Evaluation of the Soot Refractive Index in the UV-Visible from the Measurement of the Scattering and Extinction Coefficients in Rich Flames"; Combustion and Flame, v.79, pp. 259-271 (1990)
13) Klein, M. and Furtak, T; Optics, 2d ed. ; Wiley, 1986
14) Lee, S. and Tien, L.; "Optical Constants of Soot in Hydrocarbon Flames"; 18th Symposium (1981), pp 1159-1166
15) Dalessio, A. et al; " Study of the Soot Nucleation Zone of Rich Methane-Oxygen Flames"; 16th Symposium, (1976) pp. 695-708
16) Fymat, A. and Mease, K.; "Mie Forward Scattering: Improved Semiempirical Approximation with Application to Particle Size Distribution Inversion"; Applied Optics, V. 20 (2), (1981), pp. 194-198
17) Fymat, A.; "Analytical Inversions in Remote Sensing of Particle Size Distributions. 1: Multispectral Extinctions in the Anomalous Diffraction Approximation", Applied Optics, v. 17, pp. 1675-1676 (1978)
18) Fymat, A.; "Analytical Inversions in Remote Sensing of Particle Size Distributions. 2: Angular and Spectral Scattering in Diffraction Approximations", Applied Optics, v. 17, pp. 1677-1678 (1978).
19) Hodkinson, J.; "Particle Sizing by Means of the Forward Scattering Lobe"; Applied Optics, v. 5, pp. 839-844
20) Siegla, D. & Smith, G. eds.; Particulate Carbon – Formation During Combustion; Plenum Press, 1981
21) McNicholas, H; "Measurement of Fiber Diameters by the Diffraction Method"; Review of Scientific Instruments, v.2, May, 1931, pp. 263-286
22) http://en.m.wikipedia.org/wiki/Peter_Dollond, 5/2/2014
23) Eckbreth, A.; Laser Diagnostics for Combustion Temperature and Species, 2d ed; Taylor & Francis, 1996
24) Kohse-Höinghaus, K. and Jeffries, J. eds.; Applied Combustion Diagnostics; Taylor and Francis, 2002

25) Daily, J.; "Laser Induced Fluorescence Spectroscopy in Flames"; Progress in Energy and Combustion Science, v.23, pp. 133-199, 1997
26) Lapp, M. and Penney, C. – eds.; Laser Raman Gas Diagnostics; Plenum Press, 1974
27) Tolles, W. M. *et. al*.; "A Review of the Theory and Application of Coherent Anti-Stokes Raman Spectroscopy (CARS)"; Applied Spectroscopy, v. 31, pp. 253-271, 1977
28) Lal, A. & Joshi, C.; "Resonant Four-Wave Mixing of Laser Radiation in Plasmas"; Journal of the Optical Society of America B/v. 8, no 10, pp. 2148-2154, 1991
29) Yariv, A. & Pepper, D.; "Amplified Reflection, Phase Conjugation, and Oscillation in Degenerate Four-Wave Mixing"; Optics Letters, v. 1, no. 1, pp 16-18, (1977)
30) Abrams, R. & Lind, R.; "Degenerate Four-Wave Mixing in Absorbing Media"; Optics Letters, v. 2, no. 4, pp. 94-96 (1978).
31) https://www.uni-due.de/~hk0210/DFWM_Principle.HTM; "Degenerate Four-Wave Mixing (DFWM): Principle", 6/16/2014
32) Vaks, V. & Mityugov, V.; "On Relaxation Times"; Physics – Uspekhi v. 42, no. 10, pp. 1065-1066 (1999)
33) Yariv, A.; Quantum Electronics, 2d. ed. ; Wiley, 1975
34) Laurendeau, N.; "Temperature Measurements by Light-Scattering Methods"; Progress in Energy and Combustion Science, v. 14, pp. 147-170, 1988
35) Versluis, M. et. al.; "Degenerate Four-Wave Mixing with a Tunable Excimer Laser"; Applied Optics, v.33, no. 15, pp. 3289-3295
36) Drier, T. and Rakestraw, D; "Measurement of OH Rotational Temperature in a Flame Using Degenerate Four Wave Mixing"; Optics Letters, v. 15, pp. 72-74, (1990)
37) Herzberg, G.; Molecular Spectra and Molecular Structure, 1. Spectra of Diatomic Molecules; Van Nostrand, 1950
38) Herzberg, G.; Molecular Spectra and Molecular Structure, II. Electronic Spectra of Polyatomic Molecules; Van Nostrand, 1966
39) Herzberg, G.; The Spectra and Structures of Simple Free Radicals; Dover Publications, 1988
40) Pease, R. and Gaydon, A.; The Identification of Molecular Spectra, 4th ed.; Chapman and Hall, 1976
41) Kohse-Höinghaus, K.; "Laser Techniques for the Quantitative Detection of Reactive Intermediates in Combustion Systems"; Progress in Energy and Combustion Science, v. 20, pp. 203-279, 1994
42) http://orgchem.colorado.edu/Spectroscopy/irtutor/IRtheory.pdf, 6/16/2014
43) Aldén, M. *et. al*.; "Visualization and Understanding of Combustion Processes Using Spatially and Temporally Resolved Laser Diagnostic Techniques"; 33rd Symposium, pp. 69-97, 2011
44) Rothe, E. & Andresen, P.; "Application of Tunable Excimer Lasers to Combustion Diagnostics: A Review"; Applied Optics, v. 36, no. 18, pp. 3971-4033, 1997
45) Bengtsson, P. *et. al*.; "Pure Rotational CARS Measurements of Temperature and Relative O_2 Concentration in a Low Swirl Turbulent Premixed Flame"; 34th Symposium, pp. 3629-3636, 2013
46) Reichardt, T. *et. al*.; "Experimental Investigation of Saturated Degenerate Four-Wave Mixing for Quantitative Concentration Measurements"; Applied Optics, v. 38, no. 33, pp. 6951-6961, 1999

47) Hahn, J. *et. al*.; "Measuring the Concentration of Minor Species from the Modulation Dip of the Nonresonant Background of Broad-Band CARS Spectra"; Applied Spectroscopy, v. 47, no. 6, pp. 710-714, 1993
48) Buchave, P., George, W., & Lumley, J.; "The Measurement of Turbulence with the Laser-Doppler Anemometer", Annual Review of Fluid Mechanics, v. 11, pp. 443-503, 1979
49) Gupta, A., & Lilley, D.; Flowfield Modeling and Diagnostics; Abacus Press, 1985
50) Hanson, R.; "Applications of Quantitative Laser Sensors to Kinetics, Propulsion, and Practical Energy Systems"; 33rd Symposium, pp. 1-40, 2011.
51) Durrani, T., & Greated, C.; Laser Systems in Flow Measurement; Plenum Press, 1977
52) Dopheide, D. et. al.; "Three Component Laser Doppler Anemometer for Gas Flowrate Measurements up to 5500 m^3/h"; Metrologia, v. 30, pp. 453-469, 1993/1994
53) Whitelaw, J.H. et. al.; Principles and Practice of Laser-Doppler Anemometry, 2d ed; Academic Press, 1981
54) Hooker, S. & Webb, S.; Laser Physics ; Oxford University Press, 2010
55) Koelink, M.H. et al.; "Laser Doppler Velocimeter Based on the Self-Mixing Effect in a Fiber-Coupled Semiconductor Laser: Theory"; Applied Optics, v. 31, no. 18, pp. 3401-3408 (1992)
56) Edwards, R. ed.; "Report of the Special Panel on Statistical Particle Bias Problems in Laser Anemometry"; Journal of Fluids Engineering, v. 109, pp. 89-97, June, 1987
57) Eggins, P. L. *et al*; "Measurement of Mean Velocity and Turbulence in Supersonic Boundary Layers, Shock Waves, and Free Jets by Laser Anemometry"; Opto-Electronics, v. 5, pp. 91-99, (1973)
58) Kokomae, T.; "Planar Laser-Induced Fluorescence (PLIF) of H_2-O_2 Combustion"; M.S. Thesis, Aerospace Engineering, University of Texas-Arlington; August, 2003
59) http://depts.washington.edu/ntuf/facility/docs/NTUF-Raman-Tutorial.pdf, 7/5/2014
60) Unnamed authors; "Laser Anemometry, Remote Spectroscopy, and Interference"; Journal of Soviet Laser Research, 1988; v.9, no. 4, pp. 431-669
61) ISO 13320:2009; "Particle Size Analysis; Laser Diffraction Methods"; ISO standard available from the American Society for Testing and Materials, http://webstore.ansi.org/RecordDetail.aspx?sku=BS+ISO+13320%3a2009; June 22, 2013
62) Rawle, A. and Kippax, P.; "Setting New Standards for Laser Diffraction Particle Size Analysis"; American Laboratory, 1/7/2010
63) Malvern Instruments Ltd.; Mastersizer 3000 User Manual, MAN0474-06-EN-00; June 2015
64) Malvern Instruments Ltd.; Spraytec User Manual MAN0368 Issue 3.0; May 2007
65) Steinfeld, J.; Molecules and Radiation: An Introduction to Modern Molecular Spectroscopy, 2d ed; MIT Press, 1985
66) Zang, Z.; "Velocity Bias in LDA Measurements and Its Dependence on Flow Turbulence"; Flow Measurement and Instrumentation, v. 13, pp. 63-68, 2002
67) Peterson et. al.; "High-speed PIV and LIF imaging of temperature stratification in an internal combustion engine"; 34th Symposium, 2014, pp 3653-3660.
68) Lamoureux, N. et. al.; "HCN Quantitative Measurement in a Laminar Low Pressure Flame at 1036 nm Using Pulsed CRDS Technique"; 34th Symposium, 2014, pp. 3557-3564

69) Altendorfner, F. et al; "Study of the influence of electric fields on flames using planar LIF and PIV techniques"; 33rd Symposium (2011), pp. 3195-3201
70) Dworkin, S.B. et. al.; " Computational and experimental study of a forced, time-dependent, methane–air coflow diffusion flame"; 31st Symposium (2007), pp. 971-979
71) Desgroux, P., Mercier, X., Thompson, K; "Study of the formation of soot and its precursors in flames using optical diagnostics"; 34th Symposium (2013), pp. 1713-1738
72) Zheng,W. et. al; " Laser Sheet Dropsizing of Evaporating Sprays Using Simultaneous LIEF/Mie Techniques"; 34th Symposium (2013), pp. 1677-1685
73) Kempena, N., Long, M.; "Quantitative Rayleigh Thermometry for High Background Scattering Applications with Structured Laser Illumination Planar Imaging"; Applied Optics, v. 53, pp. 6688-6697 (2014)
74) Zhao, F-Q., Hiroyasu, H.; "The Applications of Laser Rayleigh Scattering to Combustion Diagnostics"; Progress in Energy and Combustion Science; v. 19, pp. 447-485, (1993)
75) Miles, R., Lempert, W., Forkey, J.; "Laser Rayleigh Scattering"; Measurement Science and Technology, v. 12, R33-R51, (2001)
76) Seasholtz, R, Buggele, A., Reeder, M.; "Flow Measurements Based on Rayleigh Scattering and Fabry-Perot Interferometer"; Optics and Lasers in Engineering, v. 27, pp. 543-570 (1997)
77) Culley, M., Jones, J., Hawk, C.; "Rayleigh Doppler Velocimetry Measurements of a Microwave Thruster"; AIAA 99-3717, 30th Plasmadynamics and Lasers Conference (1999)
78) Lock, J., Seasholtz, R., John, W.; "Rayleigh-Brillouin Scattering to Determine One-Dimensional Temperature and Number Density Profiles of a Gas Flow Field"; Applied Optics, v. 31, pp. 2839-2848, (1992)
79) Bivolaru, D. Danehy, P., Lee, J.; "Intracavity Rayleigh-Mie Scattering for Multipoint, Two-Component Velocity Measurement"; Optics Letters, v. 31, pp. 1645-1647 (2006)
80) Vaglieco, B., Beretta, F., D'Alessio, A.; "In Situ Evaluation of the Soot Refractive Index in the U.V.-Visible from the Measurements of the Scattering and Extinction Coefficients in Rich Flames"; Combustion and Flame, v. 79, pp. 259-271 (1990)
81) Holve, D., and Self, S.; "An Optical Particle-Sizing Counter for In Situ Measurements, Parts I and II"; Applied Optics, v. 18, pp 1632-1652 (1979)
82) Holve, D., and Davis, G.; "Sample Volume and Alignment Analysis for an Optical Particle Counter-Sizer and Other Applications"; Applied Optics, v.24, pp. 998-1005, (1985)